Advanced Solid-State NMR Methods for the Elucidation of Structure and Dynamics of Molecular, Macromolecular, and Supramolecular Systems

Steven P. Brown† and Hans Wolfgang Spiess*

Max-Planck-Institut für Polymerforschung, Postfach 3148, D-55021 Mainz, Germany

Received February 5, 2001

Contents

I. Introduction

In polymer science today, much interest is focused on the controlled design of well-ordered superstructures based on the self-assembly of carefully chosen building blocks. Of particular importance in this respect are noncovalent interactions,[1] e.g., hydrogen bonding and aromatic $\pi-\pi$ interactions. For example, Sijbesma et al have shown that linear polymers and reversible networks are formed from the self-assembly of monomers incorporating two and three 2-ureido-4-pyrimidone units, respectively, on account of the propensity of these units to dimerize strongly in a self-complementary array of four cooperative hydrogen bonds.[2] However, such specific interactions are not a prerequisite for a well-controlled self-assembly: e.g., as demonstrated by Percec and co-workers, the self-assembly in the bulk of dendritic building blocks into spherical, cylindrical, and other supramolecular architectures occurs as a consequence of both shape complementarity and the demixing of aliphatic and aromatic segments.[3,4]

Despite the presence of considerable order on different length scales, single crystals suitable for diffraction studies, and hence full crystal structures, are not available for such self-assembled supramolecular structures. If the mechanisms governing self-assembly are to be better understood, analytical methods capable of probing the structure and dynamics of these partially ordered systems are essential. In recent years, the field of solid-state NMR has enjoyed rapid technological and methodological development, and we will show, in this review, that advanced solid-state NMR methods are well placed to meet the challenges provided by modern polymer chemistry. In particular, much insight can be achieved for small amounts (10−20 mg) of as-synthesized samples.

The great utility of NMR lies in its unique selectivity, which is due to the differentiation of chemically distinct sites on the basis of the chemical shift. Indeed, solution-state NMR spectroscopy has developed into an indispensable method for characterizing organic molecules:[5,6] currently, one can even determine the complete three-dimensional structure of proteins of molecular masses approaching 50 kD.[7] In the solid state, however, the fast isotropic molecular tumbling that leads to the observation of inherently high-resolution solution-state spectra is absent, and anisotropic interactions, e.g., the chemical shift anisotropy (CSA), and the dipolar and quadrupolar couplings, lead to a broadening of the resonances.[8−10] These anisotropic interactions, on one hand, have the significant disadvantage of hindering the resolution of distinct sites but, on the other hand, contain valuable structural and dynamic information.

* To whom correspondence should be addressed. Tel: 00 49 6131 379120; Fax: 00 49 6131 379320; Email: spiess@mpip-mainz.mpg.de.
† Present Address: Laboratoire de Stéréochimie et des Interactions Moléculaires, UMR-5532 CNRS/ENS, Ecole Normale Supérieure de Lyon, 69364 Lyon, France.

10.1021/cr990132e CCC: $36.00
Published on Web 10/26/2001

Steven P. Brown was born in Coventry, England in 1972. He obtained a B. A. in Chemistry from Oxford University, England, in 1994. At Oxford, first as a Part II undergraduate student and subsequently for his D. Phil, which he received in 1997, he carried out research in the laboratory of Dr. S. Wimperis into NMR of half-integer quadrupolar nuclei, in particular the solid-state multiple-quantum (MQ) magic-angle spinning (MAS) experiment. From 1998 until 2000, he carried out postdoctoral research at the Max Planck Institute for Polymer Research, Mainz, Germany. Working in the group of Professor H. W. Spiess, he applied solid-state NMR methods, in particular, the combination of very-fast MAS with ^{1}H double-quantum (DQ) spectroscopy, to the investigation of structural and dynamic questions in supramolecular systems. He is currently a Marie Curie Fellow in the group of Professor L. Emsley at the Ecole Normale Supérieure, Lyon, France.

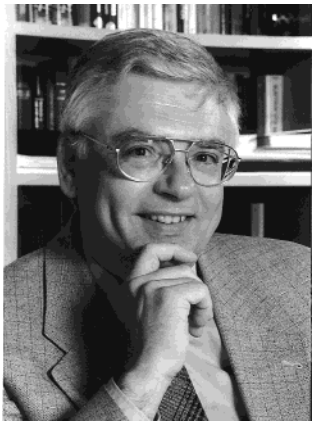

Hans Wolfgang Spiess received his Ph.D. in physical chemistry at the University of Frankfurt, Germany, with H. Hartmann in 1968. After a two year's postdoctoral stay at Florida State University with R. K. Sheline, he returned to Germany and joined the staff of the Max-Planck-Institute, Department of Molecular Physics at Heidelberg, under the direction of K. H. Hausser. In 1975, he changed to the Chemistry Department of the University at Mainz, where he became a Professor in 1978. After professorships at the Universities of Münster (1981–82) and Bayreuth (1983–84), he was appointed as a director at the newly founded Max-Planck-Institute for Polymer Research in Mainz. His main research interests are development of solid-state NMR and pulsed ESR techniques for the study of structure and dynamics of synthetic polymers and supramolecular systems.

One way by means of which the structural and dynamic information inherent to the anisotropic interactions can be probed in a site-selective fashion involves the investigation of samples where specific isotopic labels, e.g., ^{2}H, ^{13}C, ^{15}N, are introduced. ^{2}H is a spin $I = 1$ nucleus, and the quadrupolar interaction dominates ^{2}H NMR. By an analysis of one-dimensional line shapes, fast dynamic processes (10^{-4} to 10^{-7} s) can be quantitatively probed, while two-dimensional exchange experiments allow the investigation of slower motions (up to 1 s).[9] The dipolar coupling between two nuclei has an inverse cubed dependence on the internuclear separation, and, thus, solid-state NMR experiments which provide access to this interaction can be used to determine specific distance constraints. Indeed, the last 10 years have seen much interest focused on solid-state NMR experiments applicable to samples incorporating spin $I = 1/2$ isotopic labels, usually ^{13}C or ^{15}N, such that only particular dipolar-coupled spin pairs are present.[11,12] In particular, the rotational-echo double-resonance (REDOR)[13−15] technique has become very popular for determining distances between two heteronuclei, while other methods further allow the determination of torsional angles.[16,17] Although all these methods provide much valuable information, the synthetically demanding requirement for specific isotopic labeling is restrictive. Indeed, the purpose of this review is to demonstrate that much information can be obtained for as-synthesized samples, i.e., without resorting to isotopic labeling.

One of the most important recent advances in solid-state NMR has been the development of magic-angle spinning (MAS) probes capable of supporting ever greater rotation frequencies, ν_R.[18] Today, a ν_R of 25−30 kHz is routinely achievable, with an ν_R of 50 kHz even having been reported.[19] A particularly promising application for this new technology is ^{1}H solid-state NMR, where the line narrowing won by very-fast MAS alone is sufficient to allow some ^{1}H resonances due to particular chemically distinct protons to be resolved in ^{1}H MAS NMR spectra of small to moderately sized organic solids.[20−30]

The importance of solution-state NMR today owes much to the extension of the experiment to a second (and higher) dimension.[5] Multidimensional NMR spectroscopy is also of much significance in solid-state NMR: in particular, since spectral resolution is always a pertinent problem, an important motivation for performing a multidimensional experiment is the resulting increase in resolution. Indeed, a number of groups have recently developed new approaches for obtaining high-resolution two-dimensional (2D) ^{1}H-^{13}C correlation experiments.[31−33] Such experiments allow the better resolution and assignment of the ^{1}H resonances, by taking advantage of, first, the much greater resolution in the ^{13}C dimension on account of the larger chemical shift range and inherently narrower line widths, and, second, the relative insensitivity of ^{13}C chemical shifts (as compared to the case of ^{1}H chemical shifts) to through-space influences.

Multidimensional NMR experiments also provide additional information that is unavailable from one-dimensional (1D) spectra even in the limit of high-resolution. For example, 2D ^{2}H exchange experiments, which identify a particular change in molecular orientation between two evolution periods, have already been mentioned above.[9] For dipolar-coupled nuclei, the combination of fast MAS with 2D multiple-quantum (MQ) spectroscopy achieves high resolution, while allowing the structural and dynamic information inherent to the dipolar couplings to be accessed. Specifically, using the homonuclear ^{1}H-^{1}H double-

quantum (DQ) MAS experiment,[34] it has recently been demonstrated that the semiquantitative information about specific proton−proton proximities yielded by rotor-synchronized 2D spectra allows the differentiation between distinct hydrogen-bonding structures[21] as well as the identification of particular aromatic $\pi-\pi$ packing arrangements.[22,24] Moreover, it has further been shown that an analysis of rotor-encoded ^{1}H DQ MAS spinning-sideband patterns[35,36] enables the quantitative determination of the internuclear distance for a well-isolated pair of aromatic protons in a hexabenzocoronene derivative in the solid phase as well as the order parameter of the liquid-crystalline (LC) phase.[22] In addition, attention has focused on the development of methods suitable for the measurements of heteronuclear dipolar couplings between protons and other spin $I = 1/2$ nuclei (i.e., ^{1}H-^{13}C and ^{1}H-^{15}N).[37−40]

As indicated by the opening paragraphs, the emphasis of this review is on advanced solid-state NMR experiments suitable for providing insight into the mechanisms of self-assembly which are of much relevance in modern polymer science. As such, we restrict our attention to the spin $I = 1/2$ nuclei found in organic solids, in particular, ^{1}H and ^{13}C, and focus on recently developed, i.e., within the last 10 years, solid-state NMR methods that probe the structural and dynamic information inherent to the dipolar coupling. Importantly, we will show that ^{1}H NMR of rigid solids is now feasible.

We note that the considerable progress made in solid-state NMR of half-integer quadrupolar nuclei, e.g., ^{23}Na, ^{27}Al, and ^{17}O, as a consequence of the introduction of the MQMAS experiment by Frydman and Harwood in 1995,[41] falls outside the scope of this review. In addition, it is to be remembered that the NMR experiments we describe are equally applicable to biological molecules; indeed, much of the recent development of solid-state NMR methodology, e.g., the experiments for determining torsional angles,[16,17] has been stimulated by the considerable interest in biological systems. Reviewing the biological applications is, however, not an aim of this review, although a few relevant examples will be mentioned. To further specify the scope of this article, as far as the probing of dynamics is concerned, we will only consider methods suitable for probing fast processes. Thus, recently developed methods, such as one-dimensional exchange spectroscopy by sideband alternation (ODESSA),[42] time-reverse ODESSA,[43] and centerband-only detection of exchange (CODEX),[44,45] which are capable of probing slower dynamics (time scales ranging from milliseconds to seconds), will not be discussed.

To give an outline of the structure of the review, the main body is divided into two parts: first (in sections II−IV), the NMR experiments will be introduced, and, second (in sections V−VIII), specific applications will be described, which illustrate what structural and dynamic insight can be provided. These specific applications can be considered to be case studies, which illustrate how a particular system can be approached experimentally, with the methodology being extendable to other organic systems. As has been stressed above, an important aspect of this review is to highlight the importance of ^{1}H solid-state NMR—this is reflected in the chosen applications, which illustrate the valuable structural information gained on account of the marked sensitivity of the ^{1}H chemical shift to hydrogen-bonding and aromatic $\pi-\pi$ effects. In addition, the ability to probe dynamic events, such as the making and breaking of hydrogen bonds as well as guest mobility in a supramolecular complex, is demonstrated.

II. Improving the Resolution in ^{1}H Solid-State NMR

Table 1 lists the NMR-active nuclei (i.e., those with $I > 0$) of most relevance for organic solids, together with their nuclear spin quantum numbers, their magnetogyric ratios (γ), and natural abundances.[46] The low natural abundance of the nuclei ^{2}H, ^{13}C, ^{15}N explains why selective isotopic labeling is successful in these cases. Moreover, the central importance of protons in solution-state NMR is evident from Table 1: a near 100% natural abundance is combined with the highest magnetogyric ratio (and hence best sensitivity) of all naturally occurring nuclei. It is, however, exactly this combination that makes solid-state ^{1}H NMR problematic.

Table 1. Properties of the NMR-Active Nuclei of Most Relevance for Organic Solids

nucleus	I	$\gamma/10^7$ rad T^{-1} s^{-1}	natural abundance/%
^{1}H	1/2	26.8	99.99
^{2}H	1	4.1	0.02
^{13}C	1/2	6.7	1.10
^{14}N	1	1.9	99.63
^{15}N	1/2	−2.7	0.37
^{17}O	5/2	−3.6	0.04
^{19}F	1/2	25.2	100.00
^{29}Si	1/2	−5.3	4.67
^{31}P	1/2	10.8	100.00

The dipolar coupling constant, D, defining the dipolar coupling between two nuclei is given by

$$D = \frac{(\mu_0/4\pi)\hbar\gamma_I\gamma_S}{r^3} \quad (1)$$

where r denotes the internuclear separation. The dependence of D on the product of the magnetogyric ratios of the two nuclei means that the dipolar coupling constant for two ^{1}H nuclei is a factor of approximately 16 times larger than that for a pair of ^{13}C nuclei at the same separation. As an example, the ^{1}H-^{1}H D in a CH_2 group (assuming $r = 0.18$ nm) is 20 kHz, which is about twice the typically encountered chemical shift range (15 ppm) at today's largest solid-state NMR magnets (corresponding to ^{1}H Larmor frequencies of 700−800 MHz), and is much larger than the through-bond J couplings which characterize solution-state spectra.

A major difference between the *through-space* dipolar and *through-bond J* couplings is that the former is an *anisotropic* rather than an *isotropic* interaction. This means that the dipolar coupling between a pair of nuclei depends on the orientation

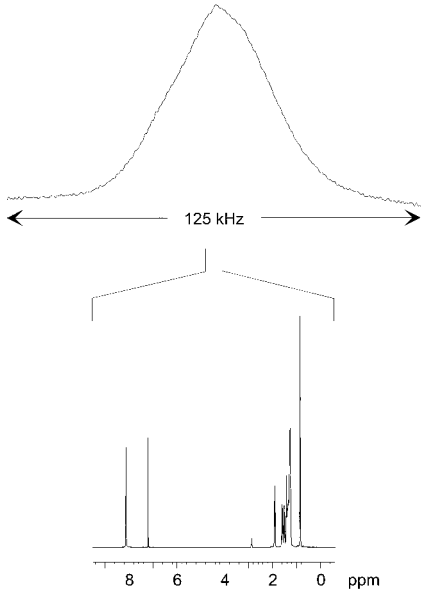

Figure 1. A comparison of the static solid-state and solution-state ^{1}H NMR spectra of a typical organic compound.

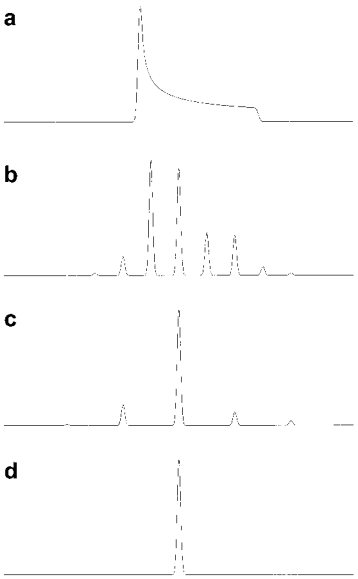

Figure 2. Simulated spectra showing the effect of MAS on the anisotropic line shape due to a CSA interaction. In (a), the sample is static, while the spectra (b) to (d) correspond to an increase in the MAS frequency, ν_R.

of the internuclear vector with respect to the direction of the static magnetic field, B_0. Specifically, the dipolar coupling is proportional to $(3\cos^2\theta - 1)$, where θ is the angle between the internuclear vector and the B_0 direction. For a powdered sample, there is a uniform distribution of orientations, and thus the NMR spectrum consists of a superposition of many lines, corresponding to the different dipolar couplings—such a powder spectrum is referred to as being anisotropically broadened.[8−10]

In organic solids, protons are ubiquitous, and an extensive network of dipolar-coupled protons exists—in so-called spin-counting experiments, clusters of over 100 dipolar-coupled protons can be identified.[47,48] As shown in Figure 1, the static ^{1}H NMR spectrum of a typical organic solid is simply a broad featureless hump. The striking difference to the corresponding ^{1}H solution-state NMR spectrum is evident. It should be stressed that the problem in the former case is not a lack of information, but rather there is essentially an overload, such that the net effect is the virtual loss of all information. The challenge facing the solid-state NMR spectroscopist is then how can experiments be designed that combine high-resolution, i.e., a recovery of the chemical shift resolution, with the preservation of the valuable information inherent to the anisotropic interactions, i.e., for ^{1}H NMR, the structural and dynamic information inherent to the dipolar coupling.

A. Magic-Angle Spinning

On account of its angular dependence, molecular motion leads to an averaging of the dipolar coupling; as will be shown later, determining the reduction in the dipolar coupling allows the identification of particular dynamic processes. The extreme case is found in solution, where fast isotropic tumbling of the molecules leads to the averaging to zero of the line broadening due to the dipolar couplings as well as the other anisotropic interactions. To achieve high resolution, the solid-state NMR spectroscopist would like to mimic this averaging process. First, we note that anisotropic interactions such as the dipolar coupling between a pair of nuclei, the CSA, and the first-order quadrupolar interaction all have an orientation dependence that can be represented by a second-rank tensor.[8−10] For such interactions, rather than requiring an isotropic motion, a physical rotation of the sample around an axis inclined at an angle of $\arctan(\sqrt{2}) = 54.7°$, the so-called magic angle, to the external magnetic field suffices.[49,50] That this is so can be understood by considering that sample rotation around a single axis leads to the components perpendicular to the rotation axis being zero on average, and only the component parallel to the rotation axis remains nonzero on average. Thus, in a powdered sample, for any orientation of, e.g., the internuclear vector for a pair of dipolar-coupled spins, rotation around an axis yields an "average orientation" parallel to the axis of rotation. Under MAS, this parallel component has an anisotropic frequency equal to zero for all cases, and the anisotropic broadening is averaged to zero for all crystallite orientations.

A familiar example of the application of MAS is ^{13}C NMR, where the combination of ^{1}H-^{13}C cross-polarization (CP)[51,52] with MAS, CP MAS NMR[53], is routinely used to investigate a wide range of systems. Under the application of high-power proton decoupling, the dominant anisotropic broadening is the CSA; in this case, as illustrated by the simulated spectra in Figure 2, the static line shape breaks up into a centerband and spinning sidebands, whose line widths are narrow and independent of ν_R. A full mathematical treatment of MAS and anisotropic interactions can be found in, e.g., refs 8, 9, 54, and 55.

The effect of MAS on a dipolar-coupled multiproton network is quite different. Figure 3 shows the effect

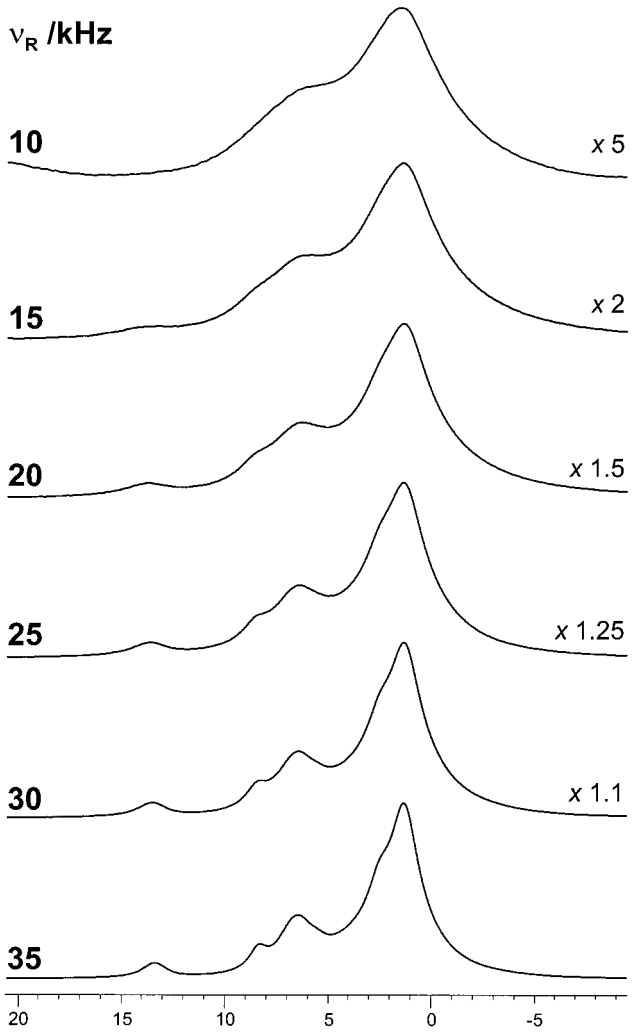

Figure 3. The effect of increasing the MAS frequency, ν_R, on the centerband of a ^{1}H MAS spectrum of a typical organic compound. (Reproduced with permission from ref 21. Copyright 1998 American Chemical Society.)

of increasing ν_R upon the centerband in the ^{1}H MAS NMR spectrum of a typical organic solid. It is apparent that the line width is not independent of ν_R, with a line narrowing being observed upon increasing ν_R—although, even at 35 kHz, the line widths are much larger than those observed in ^{13}C MAS spectra. The difference between the two cases is explained in a classic paper by Maricq and Waugh: [54] The CSA is an example of an interaction where the anisotropic broadening is refocused at the end of each rotor period, τ_R, i.e., the corresponding Hamiltonian commutes with itself at all times. By comparison, when there are three or more dipolar-coupled protons, the perturbing influence of the other dipolar-coupled protons upon a particular dipolar-coupled pair means that the dipolar Hamiltonian no longer commutes with itself at all times, and the evolution under the dipolar coupling of a particular pair is no longer refocused at the end of each τ_R.

By decreasing the rotor diameter, MAS probes capable of supporting a much faster ν_R have become available; e.g., 1997 saw the delivery of the first commercial probes designed for rotors with an outer and inner diameter of 2.5 and 1.2 mm, respectively. Such a rotor, which, when full, contains 10 mg of sample, can be spun to a ν_R of up to 35 kHz. We note that rotors with even smaller diameters, and thus smaller sample volumes, have been produced, which allow an even faster ν_R (up to 50 kHz).[19]

The enhanced line narrowing achieved by a ν_R of 30+ kHz, as compared to that obtained at a ν_R of 15 kHz (the maximum achievable with a conventional 4 mm MAS rotor), is evident in Figure 3. This line-narrowing effect, upon increasing ν_R, of MAS on the ^{1}H NMR spectrum of a dipolar-coupled proton network can be understood as being due to an increase in the spin-pair character of the interaction (the homonuclear dipolar coupling between an isolated pair of nuclei is refocusable, as in the case of the CSA).[56] As a concluding remark, we note that very-fast MAS has also been applied by Scheler to ^{19}F NMR of fluoropolymers such as PTFE; in this case, as well as achieving a line narrowing due to the reduction in the residual dipolar broadening, an additional advantage is the spectral simplification achieved by the reduction in the number of spinning sidebands (^{19}F CSAs are much bigger than ^{1}H CSAs).[57]

B. Homonuclear ^{1}H Decoupling Methods

As will be shown later, the resolution provided by the combination of very-fast MAS ($\nu_R \geq 30$ kHz) and high magnetic fields (^{1}H Larmor frequency $\geq$ 500 MHz) is sufficient to allow specific proton−proton proximities to be identified on the basis of the observation of particular peaks in ^{1}H 2D DQ MAS spectra. The line narrowing achieved by MAS alone at a ν_R equal to 35 kHz is, however, still far from the limiting case, where all residual dipolar broadening has been removed.

Brute-force fast MAS is not the only means by which line narrowing can be achieved in ^{1}H solid-state NMR. A particularly ingenious alternative approach, first presented over 30 years ago, involves the removal of the dipolar broadening by specific multiple-pulse techniques, where radio frequency (rf) pulses achieve rotations in spin space.[58,59] By combining these multiple-pulse experiments with MAS—combined rotation and multiple-pulse spectroscopy (CRAMPS)[60−62]—well-resolved ^{1}H spectra have been obtained.[63] The very time-consuming nature of the necessary setup for the CRAMPS experiment has, however, discouraged the widespread take-up of the approach. Nevertheless, recently, Hohwy et al have shown that ^{1}H CSAs can be fully determined by a CRAMPS approach employing MSHOT-3 homonuclear multiple-pulse decoupling.[64]

An important consideration in a CRAMPS experiment is the interference between the two averaging processes, i.e., does the physical rotation of the sample by MAS impair the performance of the multiple-pulse sequence, the latter having originally been designed for static samples. Indeed, a low ν_R, i.e., less than 3 kHz, is used in a conventional CRAMPS experiment, such that, to a first approximation, the sample can be considered to be static during each cycle of the multiple-pulse sequence. In this so-called "quasi-static" limit, the multiple-pulse sequence can be considered to take care of the

homogeneous dipolar broadening, with MAS being required to deal with the CSA.

Recently, Hafner and Spiess have shown that CRAMPS experiments employing a basic multiple-pulse sequence (WHH-4 or variants thereof)[58] at a moderately fast ν_R (10−15 kHz) can deliver a line narrowing corresponding to that achievable by the conventional CRAMPS approach, with a particular advantage being that the method is comparatively insensitive to experimental imperfections.[65−67] As reflected in the naming of this approach as multiple-pulse assisted MAS, such experiments represent a shift in philosophy in that both MAS and the multiple-pulse sequence "attack" the dipolar broadening; the latter can be considered to "clean up" the residual dipolar broadening, which remains as a consequence of the insufficiency of the used ν_R.

The success of the multiple-pulse assisted MAS approach requires some thought concerning the synchronization of the duration of each cycle of the multiple-pulse sequence, τ_C, with the rotor period: For the CH_3 group in L-alanine, the smallest line width (full-width at half-maximum height, fwhmh) of about 250 Hz (for comparison, the fwhmh under MAS at 35 kHz is 750 Hz)[20] is obtained for a plateau of τ_C/τ_R values between 0.2 and 0.3.[68] It has been shown that, using zero-order average Hamiltonian theory,[59,69] favorable synchronization conditions can be identified by a straightforward graphical approach.[67] The quasi-static regime is not a prerequisite for the success of multiple-pulse assisted MAS; for example, a marked line narrowing has been observed for a benzoxazine dimer using WHH-4 at 35 kHz, where τ_C/τ_R equals 1.5.[21] It is to be noted that a homonuclear decoupling method does not only remove the dipolar broadening, it also scales the isotropic chemical shift scale; all fwhmh's quoted here are those measured in a "corrected" spectrum where the normal ppm values of the different resonances have been restored.

An alternative means by which homonuclear ^{1}H decoupling can be achieved is the Lee-Goldburg experiment, in which the offset of the ^{1}H *rf* irradiation is set equal to $\omega_1/\sqrt{2}$, where ω_1 is the inherent nutation frequency of the pulse ($|\omega_1| = |\gamma B_1|$, where B_1 is the *rf* field strength), such that, in the vector model picture of NMR, the spins rotate around an effective field tilted away from the static magnetic field direction by the magic angle.[70] In this way, the zero-order average dipolar Hamiltonian vanishes. The decoupling performance is significantly enhanced in the frequency-switched Lee-Goldburg (FSLG) experiment, which involves breaking up the continuous *rf* irradiation into a series of 2π rotations of the proton magnetization about the effective field, with a switch between the two LG conditions $\pm\omega_1/\sqrt{2}$ accompanied by a simultaneous shift in the phase by π at the end of each segment.[71−73] The better performance of the FSLG method is a consequence of the setting to zero of all odd-order terms in the dipolar average Hamiltonian on account of the introduced symmetry. The FSLG method has been found to function well for a ν_R between 10 and 16 kHz,[74] with a further marked improvement being possible if the sample volume is restricted by the application of a static magnetic field gradient and a selective pulse.[75]

In the first applications of the FSLG technique, homonuclear ^{1}H decoupling was employed to remove the perturbing effects of the dipolar-coupled proton network such that, for example, the spinning-sideband patterns in a ^{13}C MAS spectrum directly reflect the heteronuclear ^{13}C-^{1}H dipolar couplings.[71,72] In addition, Levitt et al. presented a modified FSLG sequence, which, by the incorporation of acquisition windows, allowed the direct recording of high-resolution ^{1}H spectra.[73] Of more importance, however, has been the subsequent incorporation of the method into a number of experiments that achieve high-resolution in an indirect ^{1}H dimension, i.e., in cases where the FSLG irradiation does not need to be combined with direct acquisition (in this respect, the FSLG method can be termed a windowless decoupling method). For example, FSLG decoupling is an integral part of the ^{1}H-^{13}C correlation experiments presented by de Groot and co-workers[31] and Emsley and co-workers,[32] which will be described later.

Recently, Vega and co-workers have presented a phase-modulated Lee-Goldburg experiment (PMLG) experiment, in which only the phase of a series of adjacent pulses is changed, i.e., ω_1 remains constant.[76,77] In an ingenious reinterpretation of the LG concept, the zero-order term in the average Hamiltonian can be shown to vanish when the modulation of the pulse phase described by

$$\phi(t) = \omega_{PMLG} t \tag{2}$$

satisfies the condition:

$$|\omega_{PMLG}| = \omega_1/\sqrt{2}. \tag{3}$$

An LG irradiation unit has a duration corresponding to a 2π rotation of the proton magnetization about the effective field, i.e.,

$$\tau_{LG} = \sqrt{(2/3)}(2\pi/\omega_1). \tag{4}$$

Thus, the angle through which the *rf* precesses in each LG unit is given by

$$\alpha_{LG} = |\omega_{PMLG}|\tau_{LG} = 207.8° \tag{5}$$

If the sign of ω_{PMLG} is negated between alternate LG units, the symmetrization required to ensure the removal of odd-order terms in the dipolar average Hamiltonian is achieved. To demonstrate the feasibility of the PMLG sequence, Vinogradov et al employed a 2D experiment in which a high-resolution ^{1}H dimension, incorporating PMLG decoupling, is correlated with ^{1}H acquisition, with only moderate MAS (10−15 kHz) providing line narrowing in the direct dimension. The resulting resolution obtained for a sample of malonic acid is illustrated in Figure 4.[76]

Using Lee-Goldburg based decoupling methods, a fwhmh of 150−170 Hz has been reported for the aliphatic ^{1}H resonances in L-alanine[78]—this is demonstrated in part c of Figure 5, where, for comparison, the (a) static and (b) MAS (ν_R = 30 kHz) spectra are also shown. The spectrum in Figure 5c was recorded

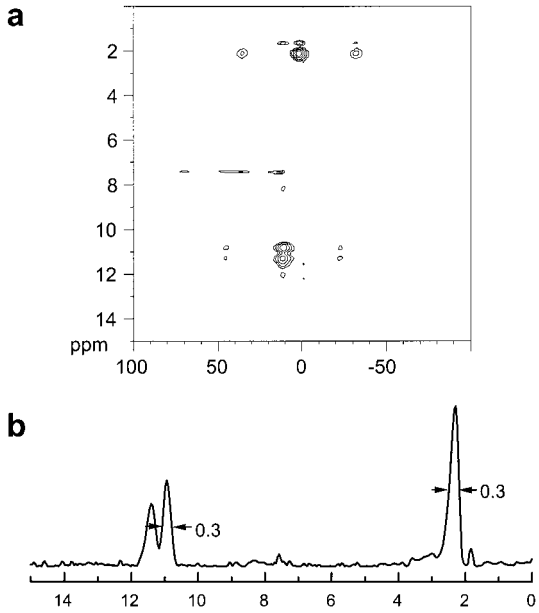

Figure 4. (a) A ^{1}H 2D PMLG spectrum of malonic acid ($(COOH)_2CH_2$). The high-resolution (F_1) projection is shown in (b), with the achieved line widths (fwhmh in ppm) being indicated. (Reproduced with permission from Figures 3a and 4a of ref 76. Copyright 1999 Elsevier.)

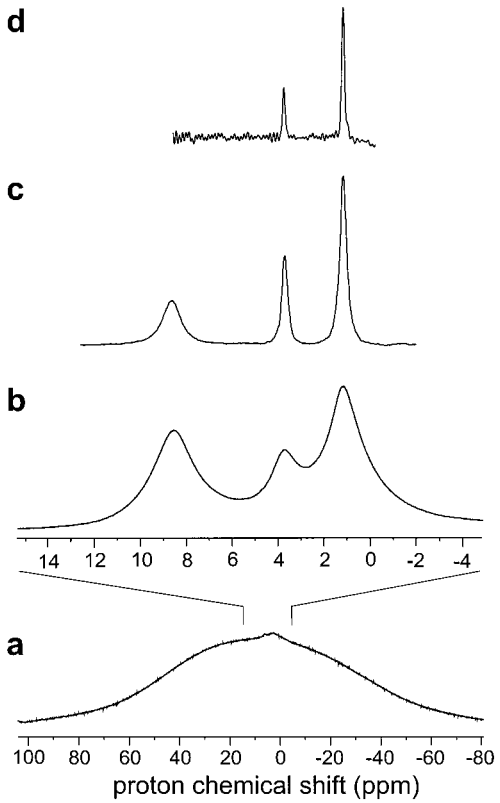

Figure 5. ^{1}H (500 MHz) NMR spectra of natural abundance powdered L-alanine, recorded with (a and b) a one-pulse experiment for (a) a static sample and (b) under MAS at a ν_R = 30 kHz, (c) the 2D FSLG (ν_R = 12.5 kHz) experiment in Figure 6a, and (d) the CT-CRAMPS (ν_R = 12.5 kHz) experiment in Figure 6b using FSLG decoupling. (Reproduced with permission from ref 78. Copyright 2001 American Chemical Society.)

using a modified version of the 2D method proposed by Vinogradov et al.[76]; as shown in the pulse sequence and coherence transfer pathway diagram[79,80] in Figure 6a, the incorporation of a *z*-filter[81] (the final two $\pi/2$ pulses) ensures that pure absorption-mode line shapes are obtained.[5,80] Lesage et al. have further shown that the frontiers of high-resolution ^{1}H solid-state NMR can be pushed back yet further: using the constant-time (CT) CRAMPS experiment shown in Figure 6b, a fwhmh as low as 60 Hz can be obtained for the aliphatic resonances in L-alanine; the achieved line-narrowing, as demonstrated in Figure 5d, is striking.[78] The success of this constant-time approach is based on the fact that the evolution of the proton magnetization in t_1 is only modulated by antisymmetric interactions, i.e., those interactions that change sign under a π rotation in spin space and are hence refocusable by a 180° pulse. The resolution enhancement over the experiment in Figure 6a is hence achieved by removing the broadening due to the symmetric interactions (those which are invariant to a π rotation); the symmetric interactions instead lead to an attenuation of the signal intensity by a factor of $\exp\{-i\mathrm{T}\mathbf{H}^{(s)}\}$.

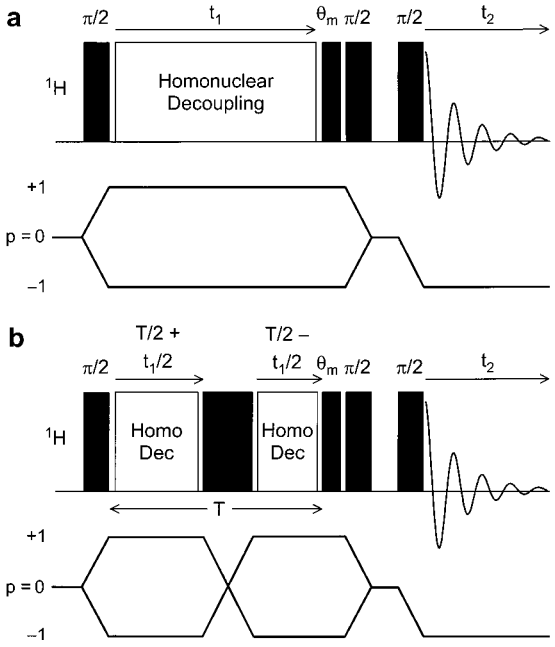

Figure 6. Pulse sequences and coherence transfer pathway diagrams for (a) a 2D CRAMPS experiment incorporating a *z*-filter to ensure that pure absorption-mode line shapes are obtained and (b) a 2D constant-time CRAMPS experiment. The relative performance of the two experiments with respect to yielding high-resolution ^{1}H NMR spectra in the indirect (F_1) dimension is illustrated by Figure 5c,d and is discussed in the text. (Adapted with permission from Figure 2 of ref 78. Copyright 2001 American Chemical Society.)

To conclude this section, it is evident that much progress has recently been made with respect to obtaining high-resolution ^{1}H solid-state NMR spectra. Indeed, the field is an area of ongoing active research, e.g., Sakellariou et al. have recently employed a computer optimization approach to develop a new homonuclear decoupling sequence, termed DUMBO-1,[82] and it is to be expected that further advances will be made in the coming years. Concerning polymer chemistry, the point is not far from being reached where the routinely achievable resolution in ^{1}H solid-state NMR is limited not by residual dipolar

broadening but rather by the inherent range of chemical shifts associated with a sample, which is not perfectly crystalline.

III. Homonuclear 2D Double-Quantum NMR Spectroscopy

The previous section has been devoted to methods that seek to achieve line narrowing in solid-state ^{1}H NMR by reducing the homogeneous broadening due to the extended homonuclear proton−proton dipolar coupling network. Such line narrowing is obviously essential to allow the resolution of distinct resonances. However, this is achieved at the expense of the loss of the valuable structural and dynamic information inherent to the dipolar coupling. A method is, therefore, required which, in addition to achieving high resolution, allows the accessing of the information inherent to the dipolar coupling. One such method is two-dimensional ^{1}H-^{1}H DQ MAS spectroscopy,[34,83] with the key to the DQ approach lying in the fact that the creation of a DQ coherence (DQC) relies on the existence of a dipolar coupling between two protons.

In solution-state NMR, many important experiments incorporate the creation and evolution of MQ coherence (MQC).[5,6,84−86] Since MQC cannot be directly detected, experiments that follow the evolution of a MQC are inherently at least two-dimensional. This is the case with ^{1}H-^{1}H DQ MAS spectroscopy. Figure 7 shows a corresponding pulse sequence and coherence transfer pathway diagram: first, a DQC is excited, which subsequently evolves during an incremented time period t_1; the DQC is then converted into observable single-quantum (SQ) coherence (SQC), which is detected in the acquisition period, t_2. To select the desired coherence transfer pathways, e.g., only DQC during t_1, a phase cycling scheme is employed.[79,80] Pure absorption-mode two-dimensional line shapes are ensured by the selection of symmetric pathways such that the time-domain

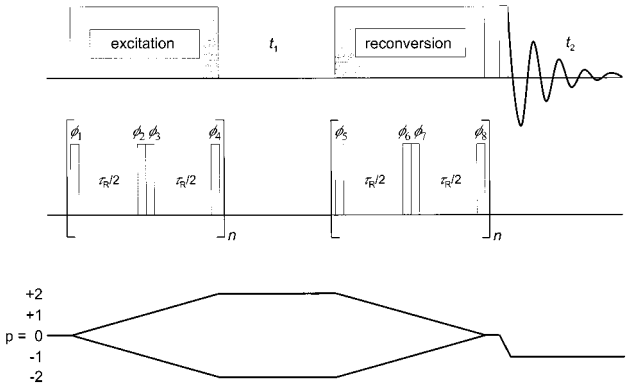

Figure 7. Pulse sequence and coherence transfer pathway diagram for a ^{1}H DQ MAS experiment using the BABA recoupling sequence for the excitation and reconversion of DQCs. The rectangular blocks represent pulses of flip angle 90°, with the choice of the phases being described in, e.g., ref 25. If the t_1 increment is set equal to a rotor period, a rotor-synchronized two-dimensional spectrum is obtained, while reducing t_1, and hence increasing the DQ spectral width, leads to the observation of a DQ MAS spinning-sideband pattern.

signal is amplitude modulated in t_1.[5,80] Sign discrimination can be restored in the F_1 dimension by the TPPI[87] or States-TPPI[88] method, which for the evolution of DQC in t_1, in both cases, involves incrementing the phases of all excitation pulses by 45° after recording each t_1 point.

A. The Excitation of Homonuclear DQC

In the solid state, the first ^{1}H MQ experiments were performed on static samples by Baum et al.;[47,48] as mentioned above, these elegant experiments allow the determination of the size of spin clusters by monitoring the time development of MQC, with average Hamiltonian theory having been used to specially design the excitation and reconversion sequences. In contrast to the homonuclear decoupling methods discussed in the previous section where it was necessary to ensure that the dipolar terms in the average Hamiltonian vanish, in this case the aim is the generation of a DQ Hamiltonian, $\mathbf{H}_{XX} - \mathbf{H}_{YY}$. In a MQ experiment, it is not enough to simply excite the MQC, attention must be paid to the careful reconversion of the MQC back to the initial state, usually longitudinal magnetization, from which directly observable transverse magnetization can be created by a single 90° *rf* pulse. For the spin-counting experiments due to Baum et al.,[47,48] a reconversion sequence which is the apparent time reversal of that used for excitation was employed, such that the destructive interference of the many MQCs is prevented.

For the excitation of DQC under MAS, the interference with the sample rotation must be considered, as was the case for the CRAMPS experiment discussed in the previous section. In particular, if a sequence designed for a static MQ experiment is used without modification, the excitation (and reconversion) time is limited to $\tau_R/2$, since the rotor modulation causes the action of the pulse sequence in the second half of the rotor period to be the time reversal of that which occurred in the first half of the rotor period. Starting with the suggestion of Meier and Earl,[89,90] who simply proposed the phase switching of the static sequences used by Baum et al.,[47,48] every half rotor period to prevent the process of self-time-reversal, many different approaches have been presented that allow excitation (and reconversion) times of one or more rotor periods. Such pulse sequences that counteract the effect of MAS are referred to as *recoupling* methods,[11,12] examples that have been used in homonuclear DQ MAS NMR spectroscopy include BABA,[91] C7,[92] DRAMA,[93] DRAWS,[94] and HORROR.[95] We note that Levitt and co-workers have recently introduced a very helpful classification system, based on symmetry principles, which covers such sequences.[96,97]

Much of the considerable effort that has been devoted to the optimization of recoupling sequences for the excitation and reconversion of homonuclear DQC has been motivated by the desire to probe weak dipolar couplings, e.g., between two specific ^{13}C labels. For ^{1}H DQ MAS NMR of rigid solids, where the dipolar couplings under consideration are usually

quite large, the demands imposed on the recoupling sequence are less severe. Moreover, to enable a ν_R of 30+ kHz to be used to obtain a sufficient line narrowing, it is important that the method is robust. In this respect, in our laboratory, we find that the BABA sequence, although it does not deliver the maximum amount of DQC, is a good candidate. As shown in Figure 7, BABA, which derives its name from the presence of back-to-back pulses, consists of segments of duration half a rotor period, where an evolution period is bracketed by two 90° pulses, with the phases of the pulses in adjacent segments being shifted by 90°. This shifting of the phases achieves a negation of the spin-part of the DQ Hamiltonian, which exactly compensates the negation of the spatial part caused by MAS. Modified two- and four-τ_R versions of the BABA sequence have also been presented, which provide compensation with respect to offset and pulse imperfections.[98] A fuller account of the operation of BABA and other recoupling sequences is found in, e.g., refs 67 and 83.

B. Rotor-Synchronized 2D DQ MAS Spectra

The two-dimensional DQ MAS experiment can be performed in two distinct ways. We consider first spectra recorded in a rotor-synchronized fashion in t_1, i.e., the t_1 increment is set equal to one rotor period, τ_R. In this way, all spinning sidebands in F_1 can be considered to fold back onto the centerband position. The appearance of a rotor-synchronized 2D ^{1}H DQ MAS spectrum is illustrated in Figure 8. Since the DQ frequency corresponding to a given DQC is simply the sum of the two SQ frequencies, DQCs between like (AA) and unlike (AB) spins can, in general, be distinguished in that, in the former case, a single peak at ($2\nu_A$, ν_A) is observed, while, in the latter case, two peaks at ($\nu_A + \nu_B$, ν_A) and ($\nu_A + \nu_B$, ν_B) are observed. [The notation (ν_1, ν_2) refers to a DQ peak centered at ν_1 and ν_2 in the F_1 and F_2 dimensions, respectively.]

To a first approximation, which is fully valid in the limit of short recoupling times and for an isolated spin pair, it can be shown that the efficiency of DQC excitation is directly proportional to the dipolar coupling constant, D.[83,99] (In this respect, a short recoupling time, τ_{rcpl}, corresponds to the case where $\sin(D\tau_{rcpl}) = D\tau_{rcpl}$). Since the reconversion to SQC efficiency has the same dependence, the integrated intensity of the DQ peaks due to a given DQC, in this limiting case, is proportional to D^2. The inverse cubed dependence of D on the internuclear distance, r, between the two nuclei means that the DQ peak intensity is inversely proportional to r^6. Therefore, by a simple inspection of which peaks are present in a rotor-synchronized ^{1}H DQ MAS spectrum, and, often more importantly, which are absent, much insight is obtained into proton−proton proximities. For example, in Figure 8a, only two of the six possible types of DQ peaks (see Figure 8b) are observed, which is consistent with the structural arrangement shown in Figure 8c. (As discussed in section VIIB, in this particular case, the inequivalence of the aromatic protons A, B, and C is a consequence of intermolecular ring current effects.) The reliability of such a semiquantitative approach has been clearly demonstrated for cases where an X-ray single-crystal structure is available to corroborate the proton−proton proximity information provided by ^{1}H DQ MAS spectra.[21,24,29] It should be noted that an advantage of the DQ approach over a spin diffusion experiment[9,100] in which a mixing time is inserted between two SQ evolution periods is that an auto (i.e., AA) peak is only observed if there is a close proximity of two protons; in the spin diffusion experiment, strong auto peaks are seen for all resonances regardless of whether there is a close proximity.

Later in this review, examples will be presented where rotor-synchronized ^{1}H DQ MAS spectra provide both structural and dynamic insight. The method is, however, not restricted to ^{1}H NMR, for example, ^{31}P-^{31}P DQ MAS spectra of inorganic phosphates and glasses have also been presented.[101−105] In addition, Nielsen et al. have presented a ^{13}C-^{13}C DQ MAS experiment,[106] using which C−C connectivities of the alkyl backbone can be established, thus, allowing the

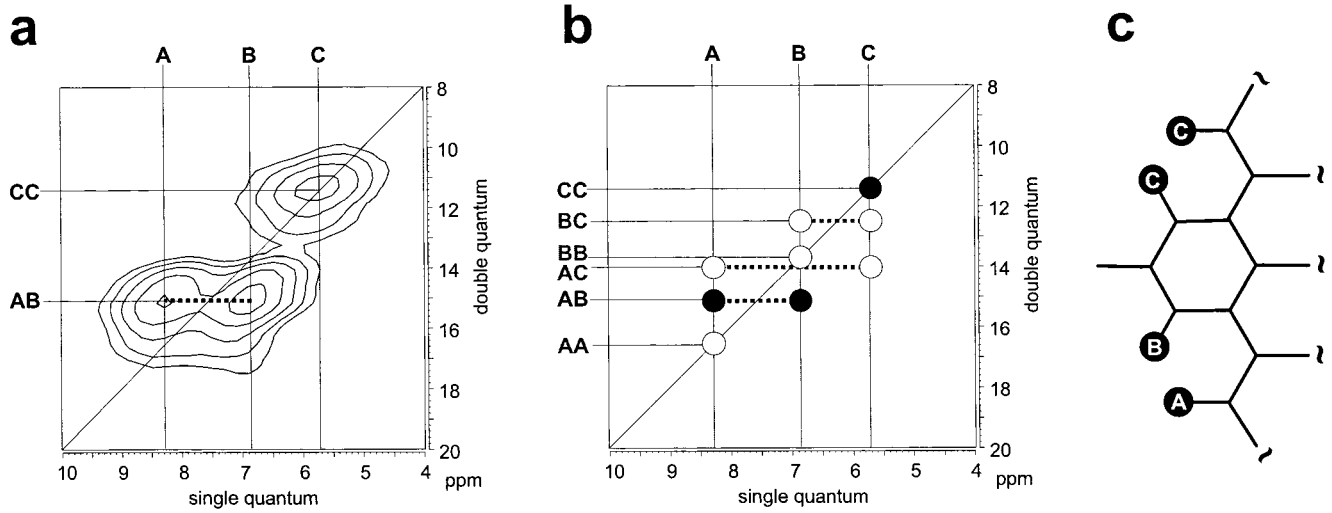

Figure 8. (a) A representative rotor-synchronized ^{1}H DQ MAS spectrum. (b) A schematic representation showing the positions of the six possible DQ peaks; the observed AB and CC peaks (filled circles) imply the proton−proton proximities indicated in (c). As discussed in section VIIB, in this particular case, the inequivalence of the aromatic protons A, B, and C is a consequence of intermolecular ring current effects. (Reproduced with permission from ref 24. Copyright 2000 Elsevier.)

assignment of the ^{13}C resonances.[87,96] In ref 107, Hong refers to the technique as the INADEQUATE experiment, which reflects the fact that the original solution-state INADEQUATE experiment due to Bax et al. creates DQC between two *J*-coupled nuclei.[108] However, an important difference between the dipolar-mediated solid-state DQ MAS experiment and the INADEQUATE experiment is that, in the latter, the use of isotropic *J* couplings for the creation of DQC means that auto peaks between spins with the same chemical shift are not observed. With regard to the information provided about through-space proximities, the DQ MAS experiment is, in fact, more similar to the solution-state NOESY experiment, the latter being heavily exploited in the structural elucidation of biopolymers.[109] Indeed, it is important to add that Emsley and co-workers have recently shown that the INADEQUATE experiment can be applied under MAS to rigid solids, with the resulting 2D spectrum identifying *J*-coupled, and hence only through-bond, correlations.[110,111]

Finally, we note that Schmidt-Rohr and co-workers have elegantly demonstrated that 2D ^{13}C-^{13}C DQ spectra recorded for static samples can identify the chain conformation statistics for ^{13}C-labeled polymer samples.[112] Remembering that the frequency of a given ^{13}C resonance depends on the orientation of the CSA tensor, the method relies on the fact that the adoption of a particular torsional angle along the chain results in DQ peaks for only specific pairs of ^{13}C frequencies. In particular, it was shown that trans and gauche conformations lead to very different 2D DQ powder spectra, and it was thus possible to quantitatively determine the conformation statistics for a sample of amorphous poly(ethylene terephthalate) (PET).

C. ^1H-^1H DQ MAS Spinning-Sideband Patterns

Rotor-synchronized ^1H DQ MAS spectra can only deliver information about relative proton−proton proximities (except for cases where the DQ peak(s) due to a known internal or external standard are well resolved).[83] The DQ MAS experiment (see Figure 7) can, however, be performed in an alternative fashion: if the t_1 increment is reduced, which corresponds to an increase in the DQ spectral width, a DQ MAS spinning-sideband pattern is observed[35,36] (provided that a recoupling sequence which has an amplitude dependence on the rotor phase, e.g., BABA[91] or DRAMA[93], is used).

The origin of such patterns is of interest, since for an isolated spin pair there is no anisotropic evolution of the DQCs during t_1 (the neglecting of the ^1H CSA implicit to this statement will be discussed later). Thus, DQ spinning sidebands cannot arise by the normal single-quantum mechanism, whereby the observed sideband pattern can be considered to map out the anisotropy of the spin interaction which is active during the evolution period. Instead, it has been shown that the origin of such spinning sidebands lies in the t_1-dependent change in the Hamiltonian active during the reconversion period relative to that active during the excitation of DQC.[35,36] This mechanism has subsequently been termed reconversion rotor encoding (RRE).[113]

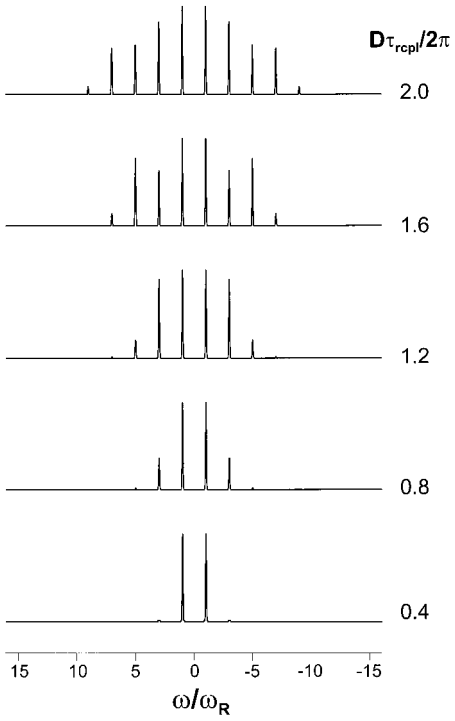

Figure 9. Simulated homonuclear DQ MAS spinning-sideband patterns generated in the time domain using eq 6, with the powder average being performed numerically, for different values of the product of D and τ_{rcpl}.

For an isolated spin pair and using $N\tau_R$ of the BABA recoupling method for both the excitation and reconversion of DQCs, the DQ time-domain signal is given by:[99]

$$s(t_1, t_2 = 0) = \langle \sin[3/(\pi\sqrt{2})D \sin(2\beta) \cos(\gamma + 2\pi\nu_R t_1)\, N\tau_R] \times \sin[3/(\pi\sqrt{2})D \sin(2\beta) \cos(\gamma) N\tau_R] \rangle \quad (6)$$

where β and γ are Euler angles relating the principal axes system of the dipolar-coupling tensor to the rotor-fixed reference frame; the $\langle\ \rangle$ brackets denote a powder average. Simulated DQ MAS spinning-sideband patterns generated in the time domain using eq 6, with the powder average being performed numerically, for different values of the product of D and τ_{rcpl} are shown in Figure 9. A particularly striking feature is that only odd-order spinning sidebands are observed; there is no intensity at the centerband and even-order sideband positions. In addition, the observed patterns are very sensitive to the product of D and τ_{rcpl}, with an increase in this product leading to the appearance of higher-order spinning sidebands. Importantly, since τ_{rcpl} is known, the absolute value of D can be extracted to a high degree of accuracy by an analysis of DQ MAS spinning-sideband patterns; in this way, as will be illustrated later, proton−proton distances as well as dynamic processes can be quantitatively determined.

In organic solids, protons rarely exist as well-isolated spin pairs. An important question that must then be asked is, what is the effect upon the observed

^{1}H DQ MAS spinning-sideband patterns of dipolar couplings to protons external to the spin pair under consideration. To answer this question, consider a model isosceles triangle three-spin system, where the distances between spins A & B, A & C, and B & C are 0.198, 0.238, and 0.238 nm, respectively, corresponding to $(D/2\pi)$s of 15.5, 8.9, and 8.9 kHz. Spins A and B, which participate in the strongest dipolar coupling, are on resonance, while spin C is 4 kHz off resonance, such that the sideband patterns due to the distinct DQCs can be resolved. Using these parameters, three-spin explicit density matrix simulations were performed, further assuming that all radio frequency pulses are infinitely short.

In Figure 10 a−c, ^{1}H DQ MAS spinning-sideband patterns for uncompensated BABA recoupling sequences of duration one, two, and four rotor periods at MAS frequencies of 15, 30, and 60 kHz in panels a, b, and c, respectively, are presented. The sideband patterns are detected at spin B; in this way, for each sideband order, the left- and right-hand peaks correspond to DQCs between spins B & C and A & B, respectively. The same line broadening (2 kHz) was applied in each case, and the narrowing of the lines is a consequence of the fact that the displayed spectral width (in kHz) doubles on going from (a) to (b), and from (b) to (c). Some phase distortions are observed for the sidebands due to the BC DQC on account of the off-resonance excitation. For comparison, Figure 10d,e presents spectra generated for a BABA recoupling sequence of duration two rotor periods at a MAS frequency of 30 kHz using the analytical time-domain formula for an isolated spin pair in eq 6, with $(D/2\pi)$s of (d) 8.9 and (e) 15.5 kHz, i.e., corresponding to the perturbing (BC) and dominant (AB) couplings in the model system.

For the three-spin simulation at a MAS frequency of 15 kHz (Figure 10a), significant intensity at the centerband and even-order spinning-sideband positions is observed. The presence of these peaks arises from the evolution during t_1 of a DQC, due to a particular two spins, under dipolar couplings to other spins; this mechanism, by means of which spinning sidebands are, in fact, most commonly generated, may be termed evolution rotor modulation.[113] On increasing the MAS frequency from 15 to 30 to 60 kHz, the intensity of the centerband and even-order spinning-sideband peaks is observed to decrease. During t_1, no recoupling pulse sequence is applied, and the averaging of the dipolar couplings to zero becomes ever more efficient upon increasing the MAS frequency, such that there is a virtual absence of centerband and even-order sideband intensity in Figure 10c.

During the excitation and reconversion of DQCs, the BABA recoupling sequence is applied, which acts against the averaging to zero of the dipolar couplings by MAS. Since the origin of the RRE mechanism is the t_1-dependent change in the Hamiltonian active during the DQ reconversion period relative to the excitation period,[113] it is to be expected that the observed odd-order sideband pattern is dependent on the perturbing dipolar couplings in a multispin system. Comparing the isolated spin-pair analytical spectra (Figure 10d,e) to the two sideband patterns in Figure 10c, it is apparent that, while the patterns for the DQC with the weaker dipolar coupling constant are quite different, i.e., the third-order sidebands are much higher for the three-spin system, the pattern for the dominant coupling in the three-spin system is only slightly different from that for the isolated spin pair. It is also important to note that the odd-order sideband pattern is virtually unchanged on doubling the MAS frequency from 30 to 60 kHz; the only change is the loss of the slight asymmetry in the first-order sidebands due to the perturbing coupling in Figure 10c. Therefore, a MAS frequency of 30 kHz suffices, as far as the determination of the limiting ^{1}H DQ MAS sideband pattern is concerned; a higher MAS frequency, though, would lead to better resolution, provided that the line broadening is due to residual dipolar couplings rather than an inherent distribution of chemical shifts.

To repeat the main conclusion, which can be reached from a consideration of the simulated DQ MAS spinning-sideband patterns in Figure 10, it is possible, for a multispin system, to determine the dominant D_{IS}, and hence the shortest proton−proton distance, to a high degree of accuracy, while the uncertainty associated with the determination of the weaker perturbing dipolar couplings is much greater. This observation is in agreement with the findings of Hodgkinson and Emsley, who concluded that the measurements of medium- to long-range C−C distances in fully labeled ^{13}C systems, i.e., the determination of a small perturbing D in the presence of a dominant D between two directly bonded ^{13}C nuclei, using homonuclear recoupling methods is prone to large errors.[114] However, unlike this ^{13}C case, where the C−C bond distance is usually not of interest, the determination of the closest proton−proton distance is often of much importance; an example concerning a complex hydrogen-bonded arrangement will be described later.

In the above discussion, the CSA has been neglected. However, at a ^{1}H Larmor frequency of 700 MHz, the CSA anisotropy parameter for hydrogen-bonded protons is nonnegligible, being approximately 10 kHz. Indeed, Tekeley et al. have shown that the CSA is responsible for distortions in the ^{1}H (300.1 MHz) DQ MAS spinning-sideband spectra obtained for barium chlorate monohydrate, $BaClO_3 \cdot H_2O$, with an excitation time of $\tau_R/2$.[115] However, these distortions manifest themselves mostly only in terms of a marked asymmetry of the lower-order sideband intensities, with the ratios of the average sideband intensities (e.g., first:third) being virtually unchanged. Furthermore, De Paul et al. have shown that including the CSA has only a minor effect on sideband patterns simulated for related rotor-encoded longitudinal magnetization (RELM) experiments, which also use BABA recoupling.[116] Thus, unless a very high degree of accuracy is required, the CSA can be safely neglected in an analysis of ^{1}H DQ MAS spinning-sideband patterns. However, for cases where the CSA is significantly bigger than the dipolar coupling, the situation is very different, e.g., as shown

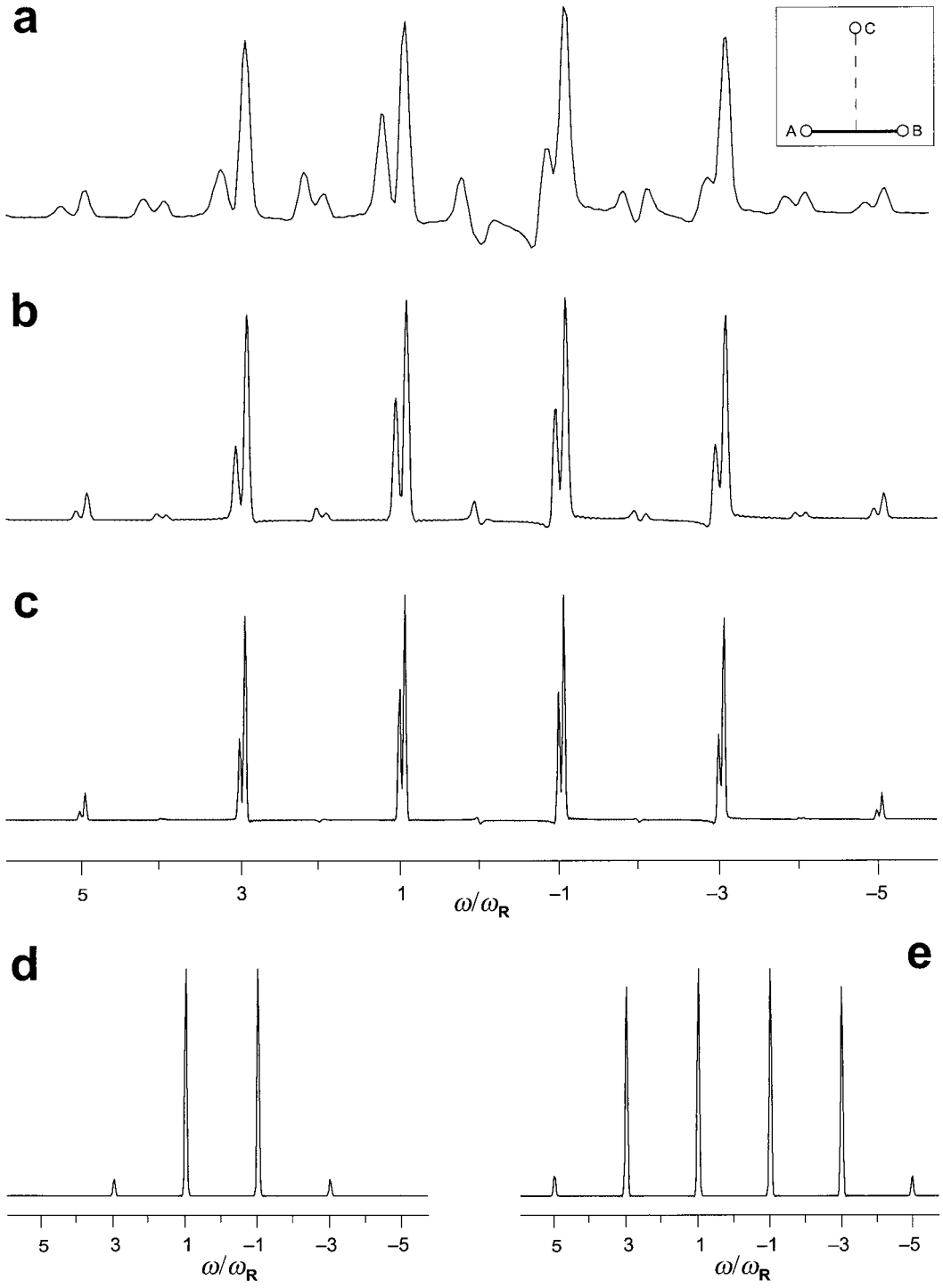

Figure 10. (a−c) Simulated ^{1}H DQ MAS spinning-sideband patterns for an isosceles triangle arrangement of three spins, where the $(D/2\pi)$s for spins A & B, A & C, and B & C are 15.5, 8.9, and 8.9 kHz (corresponding to distances of 0.198, 0.238, and 0.238 nm), respectively. Spins A & B are on resonance, while spin C is 4 kHz off resonance. The sideband patterns are detected at spin B; in this way, for each sideband order, the left- and right-hand peaks correspond to DQCs between spins B & C and A & B, respectively. Numerical density matrix simulations, assuming infinitely short radio frequency pulses, were performed for uncompensated BABA recoupling sequences of duration one, two, and four rotor periods at MAS frequencies of 15, 30, and 60 kHz in (a), (b), and (c), respectively. (d) and (e) Spectra generated using the analytical time-domain formula for an isolated spin pair, eq 6, with $(D/2\pi)$s of (d) 8.9 and (e) 15.5 kHz, for a BABA recoupling sequence of duration two rotor periods at a MAS frequency of 30 kHz. The same Gaussian line-broadening was applied for all spectra. (Reproduced with permission from ref 30. Copyright 2001 American Chemical Society.)

by De Paul et al., ^{31}P DQ MAS spinning-sideband patterns are dominated by the CSA, such that it is not possible to extract information about phosphorus−phosphorus proximities.[116] In addition, we note that Gregory et al. were able to determine the relative orientation of ^{13}C CSA tensors from an analysis of ^{13}C DQ MAS spinning-sideband patterns obtained using the DRAWS recoupling method.[117]

IV. Heteronuclear 2D NMR Methods

A. Heteronuclear Correlation Spectroscopy

When analyzing a new sample, after obtaining a rotor-synchronized ^{1}H DQ MAS spectrum, which typically only takes 1 h to record on account of the excellent sensitivity of ^{1}H NMR, one of the most important next steps is to acquire a ^{1}H-^{13}C heteronuclear correlation (HETCOR) spectrum. Such experiments allow the better resolution and assignment of the ^{1}H resonances, by taking advantage of, first, the much greater resolution in the ^{13}C dimension on account of the larger chemical shift range and inherently narrower line widths, and, second, the comparative insensitivity of ^{13}C chemical shifts to through-space influences. The enhanced sensitivity does come at a price, namely, the poorer sensitivity of ^{13}C NMR, especially at natural abundance. Nevertheless, three different methods have recently been presented, with which ^{1}H-^{13}C HETCOR spectra can be obtained in typically 8−12 h with 10−20 mg of sample at natural abundance.[31−33]

It should be emphasized that solid-state HETCOR spectroscopy is not new: as early as 1982, Caravatti et al. presented an experiment that employed a multiple-pulse sequence at a low ν_R (as in the conventional CRAMPS approach) to achieve homonuclear decoupling in t_1.[118,119] The use of this approach to obtain HETCOR spectra of range of organic solids including isotactic polypropylene and lignite,[120] as well as to investigate hydrogen bonding in amino acids and peptides[121] has been described. Moreover, the CP−WISE (wide-line separation) technique which uses the ^{13}C resolution to distinguish different mobilities as identified by the ^{1}H line width has gained popularity in polymer science.[9,122] In addition, correlation experiments are, of course, not restricted to only ^{13}C and ^{1}H; for example, Mirau et al have used ^{1}H-^{29}Si correlation experiments, namely, both an experiment incorporating ^{1}H homonuclear decoupling and a WISE experiment, to study the structure and dynamics of polymers and the water interface in porous glass composites.[123] We note that it is not our intention to give a full account of the development of solid-state HETCOR spectroscopy in this review. Indeed, our focus is on the recently developed methods, which employ fast or very-fast MAS. In this way, problems with ^{13}C CSAs, which scale linearly with the magnetic field strength, are much reduced.

The pulse sequences and coherence transfer pathway diagrams for the ^{1}H-^{13}C HETCOR experiments due to van Rossum et al. (FSLG-decoupled CP correlation),[31] Lesage et al. (MAS-*J*-HMQC),[32,124] and Saalwächter et al. (REPT-HSQC)[33,125] are shown in Figures 11, 12, and 13, respectively. The methods differ, first, in the means by which coherence transfer is achieved. The first and last approaches both make use of the heteronuclear dipolar couplings, although the use of REDOR recoupling[13−15] allows a more controlled transfer—the method is termed recoupled polarization transfer (REPT)—in the latter case as compared to the ramped CP[126] step employed by Van Rossum et al. By comparison, the method in Figure 12 developed by Emsley and co-workers utilizes the isotropic through-bond *J* coupling. Moreover, while the methods in Figures 11 and 12 use a homonuclear dipolar coupling scheme, namely, FSLG, at a moderate ν_R, to achieve narrow ^{1}H line widths, the method due to Saalwächter et al. simply makes use of brute-force very-fast MAS. As noted in section IIB, a homonuclear decoupling method causes a scaling of the isotropic chemical shift scale, which must be corrected for. For FSLG decoupling, the theoretical

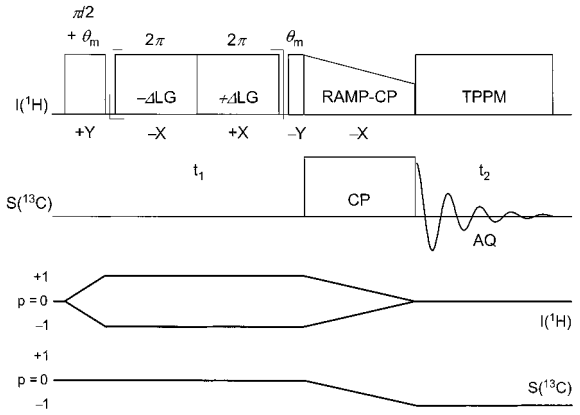

Figure 11. Pulse sequence and coherence transfer pathway diagram for the FSLG-decoupled CP HETCOR experiment, as presented in ref 31.

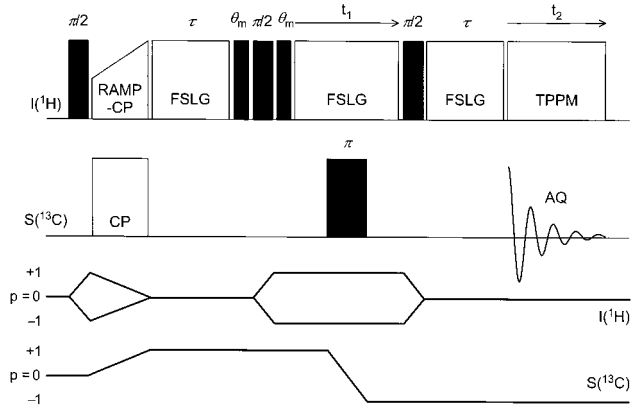

Figure 12. Pulse sequence and coherence transfer pathway diagram for the MAS-*J*-HMQC experiment, as presented in refs 32 and 124.

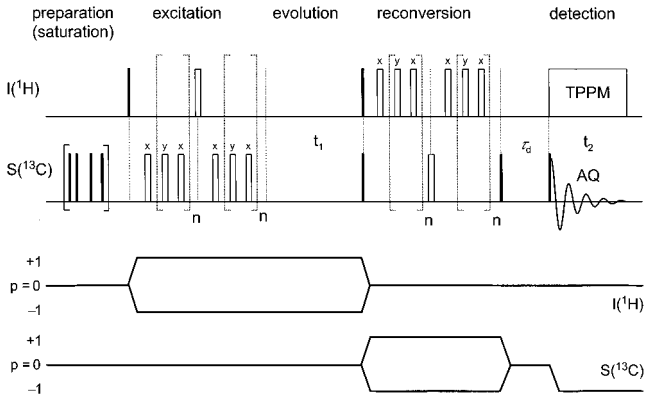

Figure 13. Pulse sequence and coherence transfer pathway diagram for the REPT-HSQC heteronuclear (^{1}H-^{13}C) experiment, which is suitable for recording HETCOR spectra. Dark- and light-shaded rectangular blocks represent *rf* pulses of flip angle 90° and 180°, respectively. For more details, see ref 125.

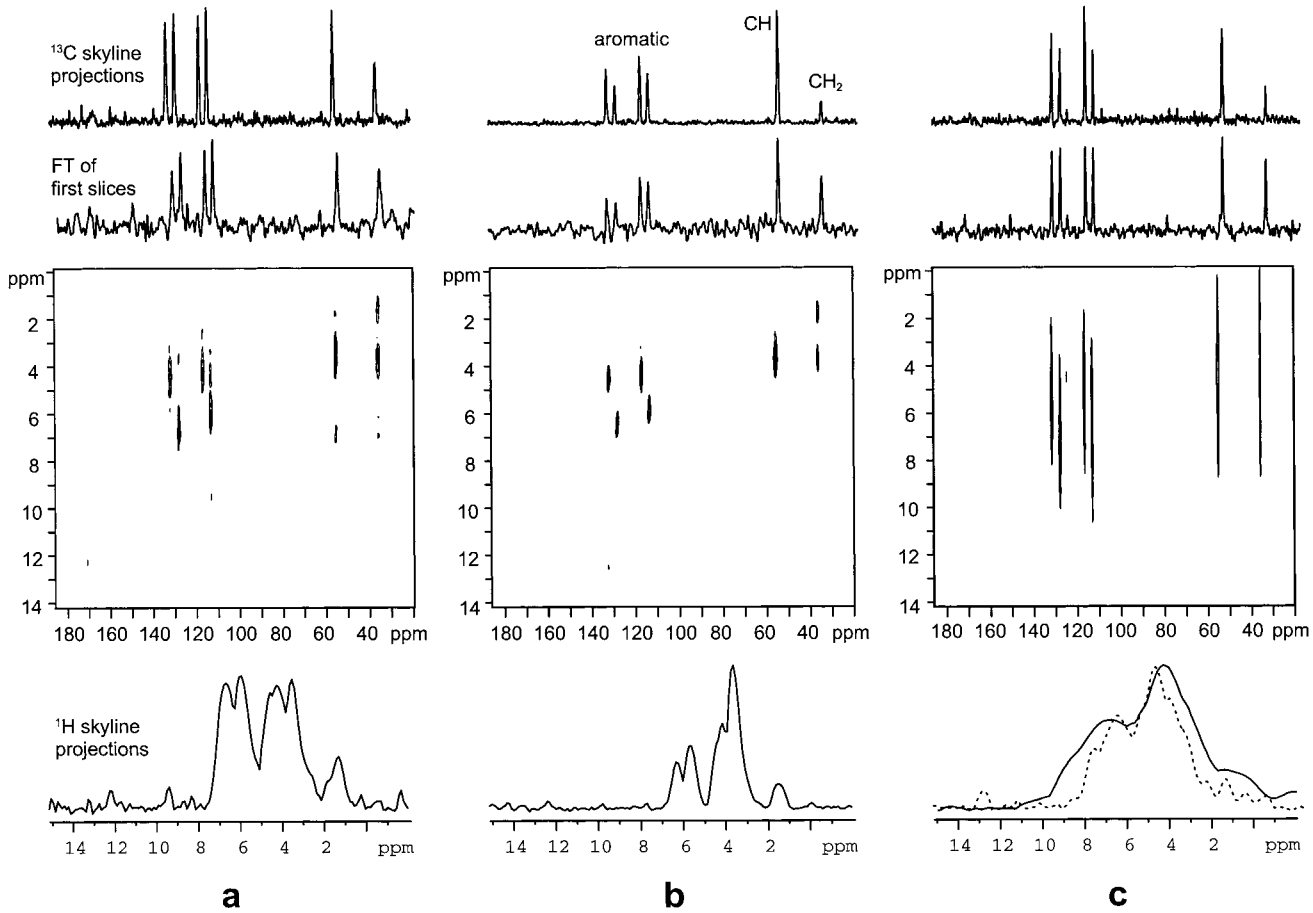

Figure 14. A comparison of three HETCOR spectra of naturally abundant L-tyrosine·HCl recorded under as far as possible equivalent conditions using (a) the FSLG-decoupled CP (Figure 11), (b) the MAS-*J*-HMQC (Figure 12), and (c) the REPT-HSQC (Figure 13) experiments. Above each spectrum, the ^{13}C skyline projection as well as the Fourier transformation of the first slice ($t_1 = 0$) of the 2D data set is shown, while below each spectrum the ^{1}H skyline projections are shown. The spectra were recorded at a ^{1}H Larmor frequency of 500 MHz; the improvement in resolution at a Larmor frequency of 700 MHz for the REPT-HSQC experiment is shown as a dashed line. (Reproduced with permission from ref 125. Copyright 2001 Academic Press.)

scaling factor is $1/\sqrt{3} = 0.58$, although, experimentally the precise scaling factor must be calibrated.

The experiments also differ with respect to the type of coherence that evolves during t_1: in Figure 11, normal ^{1}H transverse magnetization is present, while in the other two cases, heteronuclear spin modes are created, namely, heteronuclear MQC and heteronuclear SQC for the techniques in Figures 12 and 13, respectively. The analogy to the well-known solution-state heteronuclear single-quantum correlation (HSQC)[127] and heteronuclear multiple-quantum correlation (HMQC)[128] experiments (dilute-spin, e.g., ^{13}C, detected) is to be noted. We will return to the differences between the heteronuclear spin modes later. In all experiments, TPPM ^{1}H decoupling[129] is applied during ^{13}C acquisition; the better performance of TPPM over conventional continuous wave decoupling under fast MAS has been explained recently in terms of the requirement to reintroduce the homonuclear ^{1}H dipolar network to suppress the broadening due to the cross term between the heteronuclear dipolar coupling and the ^{1}H CSA.[97,130]

^{1}H-^{13}C HETCOR spectra obtained for a sample of L-tyrosine·HCl at a ^{1}H Larmor frequency of 500 MHz using the FSLG-decoupled CP (Figure 11), the MAS-*J*-HMQC (Figure 12), and the REPT-HSQC (Figure 13) experiments are presented in Figure 14panels a, b, and c, respectively. The ^{1}H line widths (fwhmh) for the FSLG-decoupled spectra are approximately 1 ppm as compared to over 3 ppm for the REPT-HSQC experiment (this does reduce to about 2 ppm at a ^{1}H Larmor frequency of 700 MHz). Moreover, Lesage and Emsley have recently shown that a fwhmh of only 150 Hz (0.3 ppm) can be obtained in a HETCOR spectrum of a sample of L-alanine recorded at a ^{1}H Larmor frequency of 500 MHz using a MAS-*J*-HSQC experiment.[131] In this respect, the experiments with homonuclear ^{1}H decoupling are superior. However, in using only very-fast MAS, it has been argued that the REPT-HSQC experiment is more robust.

The principal motivation in recording a ^{1}H-^{13}C HETCOR experiment is the determination and identification of the ^{1}H chemical shifts of the protons bound to particular carbons. For the relatively small organic molecules of relevance in modern polymer chemistry, most of the ^{13}C chemical shifts can usually be assigned by reference to the solution-state spectrum. (This is, of course, to be contrasted with the larger systems of importance in biology. A discussion of the various assignment approaches available for such systems, e.g., the ^{13}C-^{13}C correlation experi-

ments discussed at the end of section IIIB, is beyond the scope of this review.) For correlation methods based on the dipolar coupling, it is necessary to ensure that the observed peaks are then not due to close through-space proximities. In this respect, the REPT method is better than CP, although it is to be noted that van Rossum et al. have recently presented a HETCOR experiment employing LG-CP (see discussion in the following subsection).[40] This problem is obviously avoided by utilizing through-bond *J* couplings. It could be expected that the necessity for relatively long excitation periods on account of the small size of the *J* couplings would cause significant sensitivity losses. However, for the examples presented, the observed signal-to-noise is impressive; for example, the successful recording of a ^{1}H-^{15}N MAS-*J*-HMQC spectrum with ^{15}N at natural abundance has even been presented.[124] Finally, we note that the existence of methods based on both dipolar and *J* couplings opens up the possibility for distinguishing through-bond connectivities and through-space proximities on a medium- to long-range, such that insight into intermolecular packing arrangements is provided. In this way, the two approaches are complimentary in a similar way to the case of the COSY and NOESY[5,6] solution-state NMR experiments.

B. The Quantitative Determination of Heteronuclear Dipolar Couplings

A major advantage of solid-state NMR is that localized molecular motions can be quantitatively probed by the measurement of site-specific anisotropic NMR coupling parameters.[9,132] In particular, the determination of the ^{1}H-^{13}C dipolar coupling for directly bonded C−H pairs can provide much insight into, e.g., aromatic ring flips. The development of very-fast MAS and new homonuclear ^{1}H decoupling methods has led to a recent resurgence of interest in methods seeking to probe dynamics by the determination of heteronuclear one-bond dipolar couplings.

Figure 15 presents the pulse sequence for a general separated local field (SLF) experiment.[133−136] The basic principle of the SLF technique is that a spinning-sideband pattern, from which the heteronuclear dipolar coupling can be extracted, is obtained in the indirect dimension for each resolved resonance in the direct dimension, i.e., the dipolar interaction is separated from the chemical shift interaction. In the original SLF papers, a homonuclear decoupling method is applied in t_1, but recently McElheny et al.

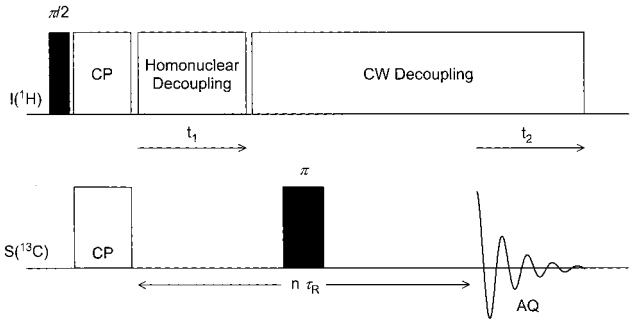

Figure 15. Pulse sequence for a conventional separated local field (SLF) heteronuclear experiment.

have shown that fast MAS alone at a ν_R of at least 12 kHz provides sufficient proton dipolar decoupling such that relatively reliable ^{1}H-^{13}C dipolar couplings can be extracted. Very-fast MAS should be avoided since the higher-order spinning sidebands become too weak to allow a reliable fitting.[39]

Alternatively, in a modification of the original SLF method, Hohwy et al. have presented a sophisticated experiment in which a pulse sequence is applied during t_1 which actively recouples the weak heteronuclear dipolar coupling while decoupling the homonuclear ^{1}H-^{1}H dipolar coupling.[38] Instead of giving a spinning-sideband pattern, a powder line shape is obtained in the indirect dimension. It is shown that this experimental approach allows the accurate determination of both N−H distances as well as the H−N−H bond angle in a NH_2 group. Another state-of-the-art method that has recently been proposed involves performing CP from ^{1}H to ^{13}C with the *rf* pulse on the ^{1}H channel fulfilling the Lee-Goldburg condition discussed earlier.[40] The suppression of the homonuclear ^{1}H dipolar couplings means that a LG-CP signal builds up in an oscillatory manner, reflecting coherent heteronuclear transfer. The Fourier transformation of such build-up curves yields powder spectra with marked singularities from the separation of which the heteronuclear dipolar coupling can be determined.

In direct analogy to the homonuclear DQ MAS experiment, if the t_1 increment in the REPT pulse sequences is not set equal to τ_R, a spinning-sideband pattern rotor-encoded by the heteronuclear dipolar coupling is obtained.[33,37,125] In Figures 13 and 16, two alternative implementations of the REPT experiment are presented, which can be seen to differ as to where, with respect to t_1, the second and third 90° pulses are applied. In both cases, the evolution of transverse ^{1}H magnetization, $-I_y$, under the heteronuclear dipolar coupling gives at the end of the first REDOR recoupling period a heteronuclear SQC, $2I_xS_z$. In the REPT-HSQC experiment in Figure 13, there are no pulses before the start of the t_1 period; as illustrated in the previous subsection, this variant is suitable for a HETCOR experiment, since only ^{1}H transverse magnetization evolves during t_1.

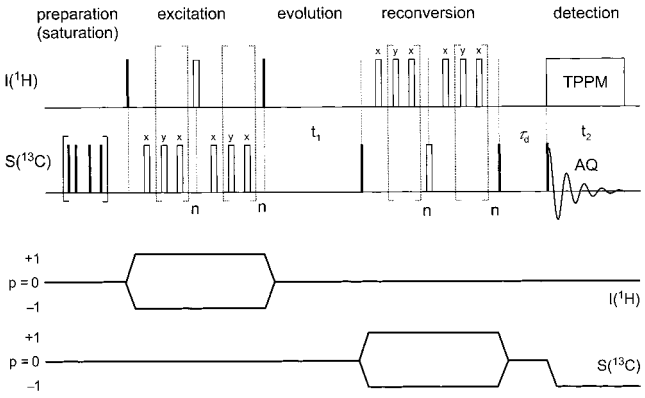

Figure 16. Pulse sequence and coherence transfer pathway diagram for the REPT-HDOR heteronuclear (^{1}H-^{13}C) experiment, which is suitable for recording rotor-encoded spinning-sideband patterns. Dark- and light-shaded rectangular blocks represent *rf* pulses of flip angle 90° and 180°, respectively. For more details, see ref 125.

In Figure 16, a ^{1}H 90° pulse is applied before t_1 to give a state of heteronuclear dipolar order, $2I_zS_z$, which does not evolve under either the ^{1}H or ^{13}C chemical shift during t_1. This experiment is suitable for recording rotor-encoded spinning-sideband patterns without any distortions from chemical shift evolution. It is referred to as REPT-HDOR (heteronuclear dipolar order rotor encoding). In most cases, the loss of chemical shift information in the ^{1}H dimension is not a problem. An advantage of the REPT-HDOR approach is that it is only necessary to record the t_1 signal for one τ_R; the acquired signal can then be catenated and multiplied by a weighting function to introduce an artificial line broadening before Fourier transformation. The heteronuclear REPT spinning-sideband patterns for a heteronuclear spin pair are identical to those shown in Figure 9 for DQ MAS of a homonuclear spin pair except for a factor of 1.5 which reflects the difference in the homonuclear and heteronuclear dipolar Hamiltonians.

If a ^{13}C 90° pulse is applied before t_1 a heteronuclear MQC, $2I_xS_x$, is obtained. Indeed, this REPT-HMQC experiment is described in the original paper.[33] The disadvantage in this case is that, to record a HETCOR experiment, a 180° pulse must be applied in the center of t_1 to refocus the ^{13}C chemical shift evolution. Note the presence of such a pulse in the MAS-*J*-HMQC experiment in Figure 12. The inclusion of this 180° pulse leads to a timing problem;[125] however, Lesage and Emsley have recently shown that the insertion of a 180° pulse in the center of t_1 leads to a better resolution in a HSQC experiment on account of the refocusing of the heteronuclear *J* and residual dipolar couplings.[131] Finally, it should be mentioned that a related set of experiments, termed dipolar heteronuclear multiple-spin correlation (DIP−HMSC), have recently be described, which also incorporate REDOR recoupling but begin with ^{13}C transverse magnetization created by a CP step.[137]

V. Structural Determination by Solid-State NMR

In polymer science, an understanding of the relationship between microscopic structure and macroscopic properties is essential for an intelligent design of new improved materials. In this section, we present some case studies that illustrate the role which solid-state NMR can play with regard to the determination of the microscopic structure. It is first necessary to consider how solid-state NMR relates to other methods for structural determination, in particular the established scattering methods. For solids, for which a single crystal of suitable size can be obtained, the ability of X-ray or neutron diffraction methods to determine the complete three-dimensional structure with atomic resolution cannot be matched.

The proven power of the single-crystal diffraction techniques does not, however, make solid-state NMR irrelevant. In materials science, most samples do not possess long-range translational order, and it is not possible to prepare single crystals. Such samples are, however, usually well-ordered on a local scale. The solid-state NMR methods introduced in the previous sections are all designed for application to powdered samples, i.e., there is no requirement for a single crystal. The ability of solid-state NMR to provide structural information about partially ordered samples will be demonstrated in this section. In this respect, we note that the analysis of solid-state NMR spectra obtained for samples where it was not possible to prepare a single crystal suitable for X-ray diffraction is greatly aided by the existence of X-ray or neutron single-crystal structures of related systems.

Solid-state NMR is also not redundant for the case where it is possible to prepare a single-crystal suitable for an X-ray analysis, since structure determination by single-crystal X-ray diffraction methods, being based on the diffraction of X-rays by electrons, is not well suited to the localization of lighter atoms. This is of particular relevance with regard to the localization of hydrogen-bonded protons, in which case a neutron diffraction study is to be preferred.[138] It should be noted, though, that neutron diffraction is not the perfect solution: as well as the requirement for both larger crystals and very expensive facilities, the investigation of protons is complicated by their large incoherent cross section, such that deuteration, which may cause a change in the hydrogen-bonding arrangement, is often required. Thus, solid-state NMR methods that can provide interproton and proton−heteroatom distance constraints, by means of which the localization of the important protons in the single-crystal structure can be refined, are of much value.

In addition, solid-state NMR is well-suited to an investigation of polymorphism. In this respect, it is to be remembered that, when selecting single crystals suitable for a diffraction study, it could happen that minor crystalline forms, which may less readily form single crystals, are missed. For example, using a modified version[139,140] of the magic-angle turning (MAT)[141] experiment, which allows the separation of ^{13}C CSA tensor spinning-sideband patterns, Harper and Grant were able to assign the observed ^{13}C resonances to different polymorphic forms of the terpene verbenol.[142] In this case, single crystals suitable for an X-ray diffraction analysis could only be obtained for the major crystalline form.

To summarize: solid-state NMR should not be considered as a replacement for the established scattering methods. Instead, the two methods should be thought of as being complementary, since they have much to offer each other.

VI. Hydrogen-Bonded Systems

To investigate hydrogen bonding by solid-state NMR, the obvious nuclei to investigate are either ^{1}H or ^{2}H. Considering ^{1}H NMR, the components of the ^{1}H CSA tensors of the hydrogen bonded protons in a number of compounds, in particular carboxylic acids, have been determined for static single crystals using multiple-pulse dipolar decoupling methods. For a general hydrogen bond O−H···O, a clear correlation between the ^{1}H isotropic chemical shift and the hydrogen-bond strength as given by the O···H and O···O distances determined by single-crystal diffraction studies has been established.[143−145] These studies

also established a corresponding correlation with the ^{2}H quadrupolar coupling constant, as determined from the powder line shapes obtained for deuterated samples. In this section, we show that the advanced ^{1}H solid-state NMR methods available today yield much structural information about complex hydrogen-bonding arrangements, without requiring either a single crystal or isotopic labeling. In particular, the shifting of hydrogen-bonded resonances well away from the aliphatic peaks means that solid-state ^{1}H NMR methods are ideally suited to the investigation of what is often the most interesting part of the structure.

A. Rotor-Synchronized ^{1}H DQ MAS NMR Spectroscopy

As a first example, we show how rotor-synchronized ^{1}H DQ MAS spectra can distinguish between the solid-state hydrogen-bonded structures adopted by two different alkyl-substituted benzoxazine dimers [*N*,*N*-bis(3,5-dimethyl-2-hydroxybenzyl) "R" amine, where "R" = methyl or ethyl], **1**, in the solid state.[21]

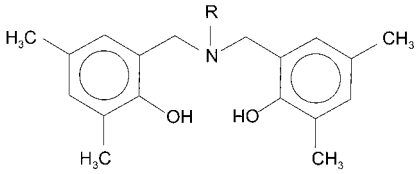

1

These dimers are of interest because they serve as model compounds for a new class of phenolic materials, the polybenzoxazines, whose synthesis and characterization has been described by Ishida and coworkers.[146−149] These polybenzoxazine resins were found to have a number of unusual, but commercially favorable, properties, in particular a near-zero shrinkage or volumetric expansion upon curing (polymerization) as well as low water absorption. In addition, the resins have high glass-transition temperatures even though they have been shown to have low crosslink densities. Explanations for these properties have been hypothesised in terms of favorable hydrogen-bonding interactions.[150]

In Figure 17a, the 1D ^{1}H (500.1 MHz) MAS (ν_R = 35 kHz) spectra of the methyl (solid line) and ethyl (dashed line) dimers are superimposed. Note that the spectra demonstrating the resolution enhancement effect of increasing the ν_R in Figure 3 were for this ethyl benzoxazine dimer. Of most importance are the clear differences between the two spectra in the low-field region, which corresponds to the hydrogen-bonded protons. For the ethyl dimer, in addition to the peaks due to the aliphatic and aromatic protons, two resonances at 13.2 and 8.2 ppm can be identified. By comparison, for the methyl dimer, a single peak at 11.2 ppm, together with a shoulder at 7.2 ppm (this peak is better resolved in the ^{1}H 2D DQ MAS spectrum − see below), is observed. The change of a single substituent from methyl to ethyl would not be expected to change the affinity of the amine nitrogen

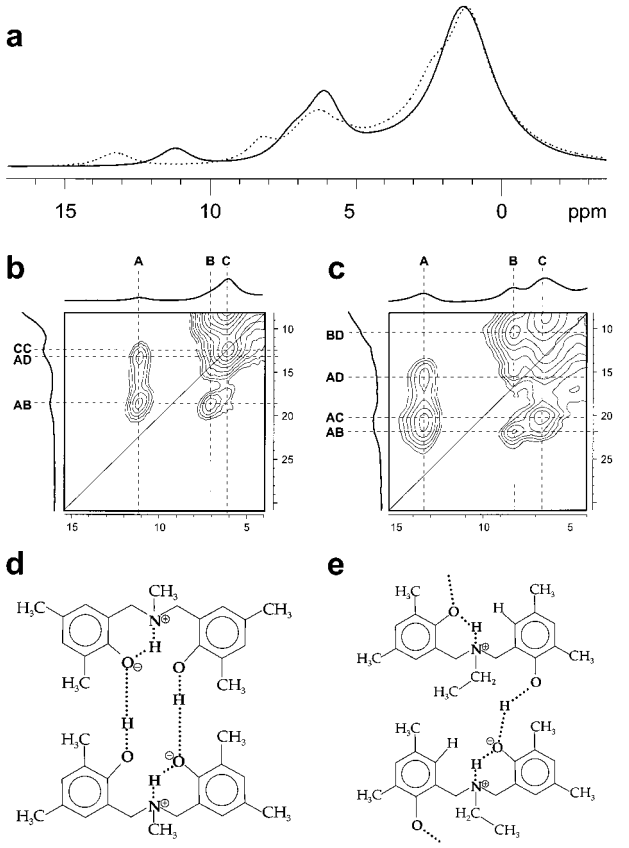

Figure 17. (a) The ^{1}H (500.1 MHz) MAS (ν_R = 35 kHz) spectra of the methyl (solid line) and ethyl (dashed line) benzoxazine dimers, **1**. (b, c) The low-field regions of rotor-synchronized ^{1}H DQ MAS spectra of (b) the methyl and (c) the ethyl dimers. (d, e) Schematic representations of the proposed arrangement of (d) the methyl dimers into pairs, and (e) the ethyl dimers into a chainlike structure. (Adapted with permission from Figures 1, 5, 6, 8, and 9 of ref 21, Copyright 1998 American Chemical Society.)

to protons to the extent that would be necessary to explain a 2 ppm low-field shift of the most low-field resonance. Instead, lengthening the *N*-alkyl chain seems to induce a more profound change in the arrangement of the hydrogen bonds.

Figure 17b,c shows the low-field regions of rotor-synchronized ^{1}H 2D DQ MAS NMR spectra recorded for the methyl and ethyl dimers, respectively. The labels A & B, C, and D refer to the SQ resonances of the hydrogen-bonded, aromatic, and aliphatic protons, respectively. For the methyl dimer, an X-ray single-crystal structure exists,[151] which indicates that the dimers form themselves into pairs. This X-ray study was, however, not able to locate the positions of the vital hydrogen-bonded protons. Figure 17d presents a schematic representation of a pair of methyl dimers linked by an extended hydrogen-bonded arrangement, the latter having been proposed on the basis of molecular modeling results.

The validity of the structural model in Figure 17d is proven by the ^{1}H DQ MAS spectrum in Figure 17b. First, the observation of two hydrogen-bonded resonances is explained: A and B correspond to the O−H···N and O−H···O protons, respectively (this assignment is on the basis of CRAMPS spectra and also results subsequently obtained for a ^{15}N labeled sample). Remembering that a DQ peak is only

observed if the two protons have a close through-space proximity, the observation of a strong AB cross-peak and the absence of an AA auto peak is consistent with the extended hydrogen-bonded arrangement in Figure 17d. The presence of a strong CC auto peak is interesting: for an isolated pair of dimers, there are no two nearby aromatic protons that are close enough to explain this observation; rather, the crystal structure indicates a close approach of aromatic protons belonging to different pairs of dimers.

Although the ^{1}H DQ MAS spectrum of the ethyl dimer in Figure 17c is similar to that of the methyl dimer in Figure 17b, for example, a clear AB cross-peak between the O−H···N and O−H···O protons can be identified, so providing evidence for the same type of extended N···H−O···H−O hydrogen-bonded link in both samples, there exist some profound differences. The most striking differences between the methyl- and ethyl-dimer spectra are, while for the methyl dimer, there is a strong aromatic auto peak (CC) and only weak intensity corresponding to a DQC between a O−H···N and an aromatic proton (AC), the situation is reversed for the ethyl dimer. As discussed above, the strong aromatic auto peak in the methyl dimer is due to the close proximity of two aromatic protons of two different hydrogen-bonded dimer pairs, and the clear difference in the ethyl spectrum therefore indicates an alternative packing arrangement.

A consideration of the basic structure of the benzoxazine dimer reveals that the observation of both the strong AC peak and the absence of the CC peak for the ethyl dimer can be explained if one of the aromatic rings is flipped such that instead of pairs of hydrogen-bonded dimers there exist hydrogen-bonded chains as shown in Figure 17e. In addition, this alternative packing arrangement gives rise to a close proximity of the O−H···O proton and the *N*-ethyl chain. The resulting cross-peak between the O−H···O proton and the ethyl-chain CH_2 protons (BD) is, indeed, clearly seen in the DQ MAS spectrum of the ethyl dimer (Figure 17c).

A further example of the utility of rotor-synchronized ^{1}H DQ MAS NMR spectra is the investigation of the change in the quadruple hydrogen-bonding arrangement formed by dimers of 2-ureido-4-pyrimidone units upon a keto to enol tautomerism.[83,152] The ability of monomers incorporating two and three of these units to self-assemble into linear polymers and reversible networks, respectively, was noted in the Introduction.[2] In an additional related example focusing on ionic intermolecular interactions, Rodriguez et al. have presented 2D rotor-synchronized ^{1}H DQ MAS spectra that prove the intimate contact of the two polymers, poly(sulfonated styrene) (PSS) and poly(diallyldimethylammonium chloride) (PDADMAC), in both a polyelectrolyte complex and thin self-assembled PSS/PDADMAC multilayers on silica colloids.[26]

B. ^{1}H DQ MAS NMR Spinning-Sideband Patterns

The rotor-synchronized ^{1}H DQ MAS experiment can be considered to be a workhorse method; valuable semiquantitative insight is provided by the straightforward interpretation of spectra that typically require less than 1 h of measuring time. The recording of ^{1}H DQ MAS spinning sideband patterns usually requires a significantly longer measuring time (8−12 h). However, as illustrated by the following examples, the extra investment is often rewarded by additional important structural information.

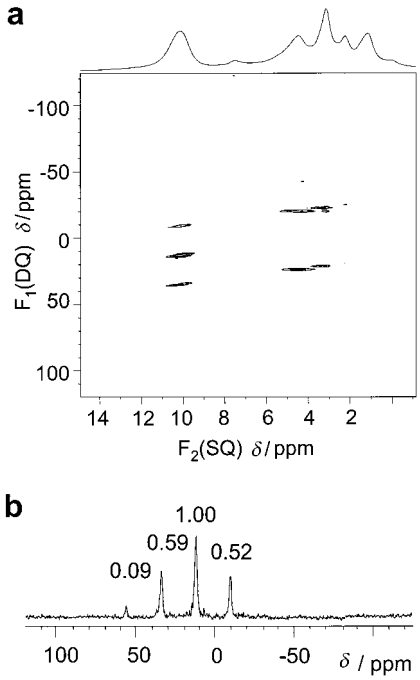

Figure 18. (a) A 2D ^{1}H (500.1 MHz) DQ MAS spectrum of an all-silica ZSM-12 zeolite. The spectrum on top is the ^{1}H MAS spectrum. (b) The ^{1}H DQ MAS spinning-sideband pattern for the SQ resonance at 10 ppm, corresponding to the hydrogen-bonded protons. (Reproduced with permission from Figures 4 and 5 of ref 153. Copyright 2000 American Chemical Society.)

As noted above, the presence of centerband and even-order sideband intensity in a ^{1}H DQ MAS spectrum arises from the evolution during t_1 of a DQC, due to a particular two spins, under dipolar couplings to other spins. In an elegant use of this phenomenon, Shantz et al have shown how the observation of an intense centerband in the ^{1}H DQ MAS spinning-sideband pattern for the SQ resonance at 10 ppm—see Figure 18 —proves that at least three silanol protons are engaged in hydrogen bonding within the defect sites in an all-silica ZSM-12 zeolite.[153]

The simulated spinning-sideband patterns for a model three-spin system presented in Figure 10 demonstrated that at a very-fast ν_R, i.e., 30+ kHz, the evolution during t_1 of a DQC under perturbing dipolar couplings to other spins is suppressed, such that the intensity of the centerband and even-order sidebands is usually weak. In addition, Figure 10 showed that the effect of a perturbing dipolar coupling on the odd-order spinning-sideband pattern generated by the RRE mechanism for the DQC corresponding to the dominant *D* is small, such that it is possible, for a multispin system, to determine the dominant *D*, and hence the shortest proton−proton distance, to a high degree of accuracy. As an explicit example of this, consider the hydrogen-

bonded arrangement in bilirubin IXα (henceforth referred to simply as bilirubin), **2**.[30]

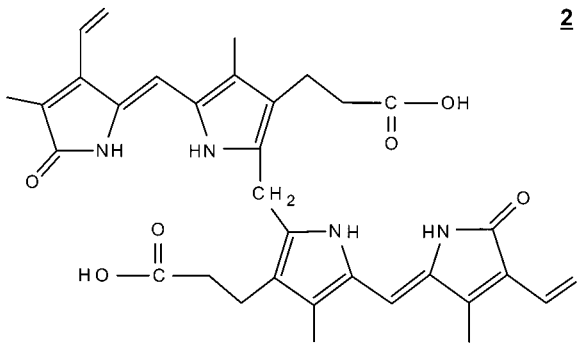

Bilirubin is an unsymmetrically substituted tetrapyrrole dicarboxylic acid, which is found in the body as a product of the metabolism of hemoglobin from red blood cells.[154] Bilirubin itself is intrinsically unexcretable, and its removal from the body requires it first to be conjugated enzymatically with glucuronic acid in the liver. An insufficient elimination of the yellow-orange pigment, bilirubin, results in hyperbilirubinemia, which manifests itself as jaundice; such a condition is usually associated with a pathologic liver disease, e.g., hepatitis, or an insufficiency of the bilirubin glucuronyl transferase enzyme, the latter being commonly the case in newly born infants.[155]

On account of its medical importance, much effort has been devoted to the investigation of the structure of bilirubin. X-ray single-crystal studies have demonstrated that bilirubin crystallizes in the solid-state with the ridge-tile-shaped conformation illustrated in Figure 19: the two halves of the molecule can be considered to be planar tiles, aligned at an angle of approximately 100° with respect to each other.[156,157] The crystal structure indicates that the carboxylic acid group of one dipyrrinone unit adopts an ideal geometry for intramolecular hydrogen bonding with the lactam and pyrrole moieties of the other dipyrrinone unit. The involvement of the carboxylic acid groups in strong intramolecular hydrogen bonding renders bilirubin effectively insoluble in aqueous solution.

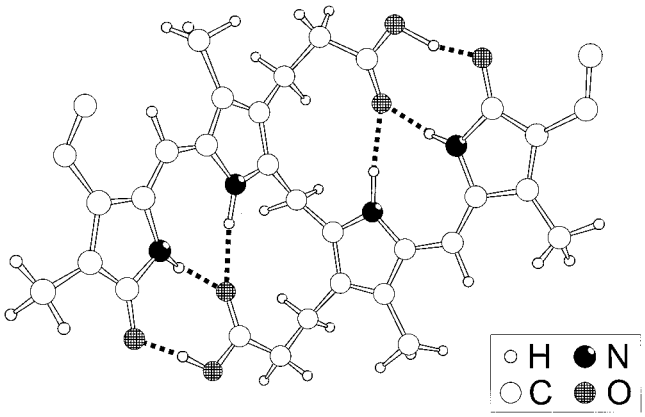

Figure 19. The structure adopted by bilirubin, **2**, in the solid state, as determined by an X-ray single-crystal diffraction study.[157] The intramolecular hydrogen-bonding arrangement is indicated. (Reproduced with permission from ref 30. Copyright 2001 American Chemical Society.)

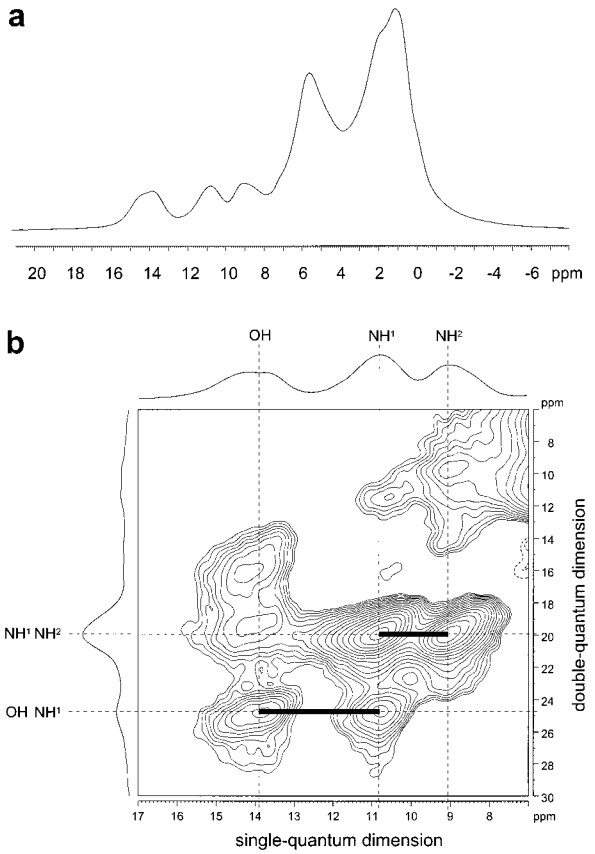

Figure 20. (a) ^{1}H (700.1 MHz) MAS (ν_R = 30 kHz) NMR spectrum of bilirubin, **2**. (b) The part corresponding to the hydrogen-bonded resonances of a rotor-synchronized ^{1}H DQ MAS NMR spectrum, together with skyline SQ and DQ projections, of bilirubin, **2**. (Reproduced with permission from ref 30. Copyright 2001 American Chemical Society.)

As stated above, the exact localization of protons by X-ray scattering is very difficult. Indeed, in the first X-ray single-crystal study,[156] the positions of the vital hydrogen-bonded protons were very poorly defined. Furthermore, although Le Bas et al. went to considerable trouble to obtain a single crystal of suitable quality to allow the location of the hydrogen-bonded protons, they were still forced to artificially calculate the position of one of the three hydrogen-bonded protons in each half of the bilirubin molecule.[157] There is, therefore, likely to be a significant uncertainty in the proton−proton distances derived from the X-ray structure.

Figure 20a presents the 1D ^{1}H MAS spectrum of bilirubin, recorded at a ^{1}H Larmor frequency of 700.1 MHz and a MAS frequency of 30 kHz. Three low-field resonances can clearly be resolved. In Figure 20b, the part of a 2D rotor-synchronized ^{1}H DQ MAS spectrum corresponding to these hydrogen-bonded resonances is shown. Only the proton corresponding to the middle hydrogen-bonded peak at 10.8 ppm can then be seen to be in close proximity to both the other two hydrogen-bonded protons. By reference to the intramolecular hydrogen-bonded arrangement known from the single-crystal X-ray investigation (see Figure 19), the peak at 10.8 ppm can then be assigned to the lactam NH proton. The solid-state ^{1}H chemical shifts are very similar to the solution-state values obtained using chloroform as a solvent, where there

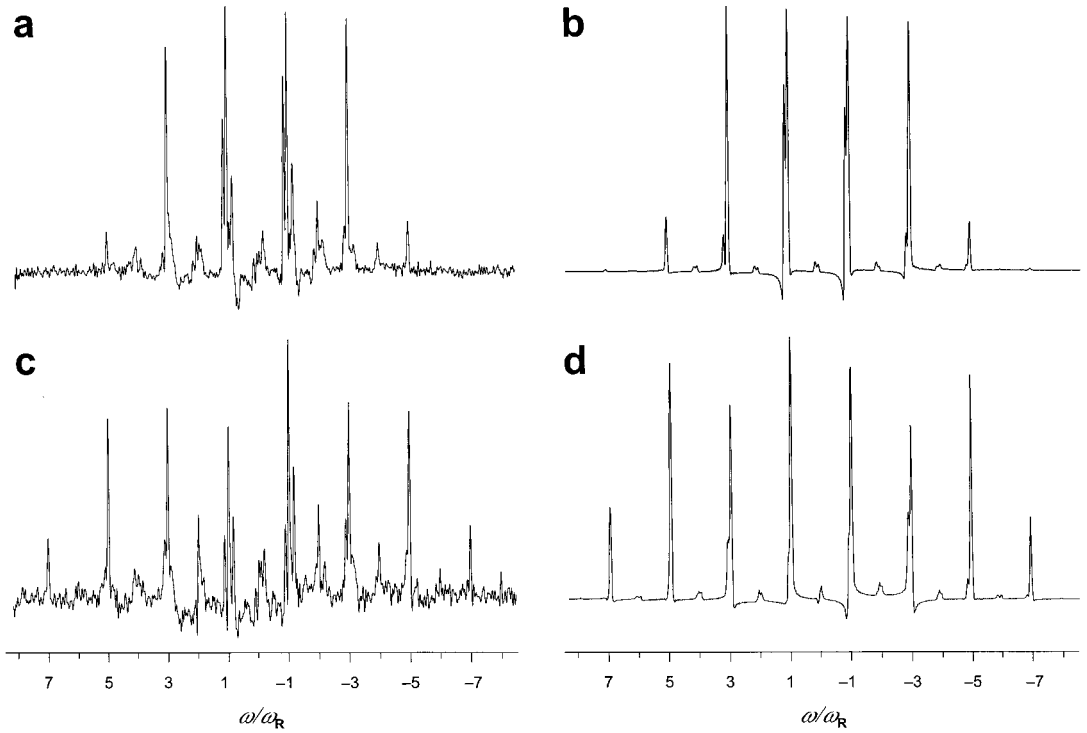

Figure 21. (a, c) ^{1}H (700.1 MHz) DQ MAS NMR spinning-sideband patterns obtained for the NH[1] hydrogen-bonded resonances of bilirubin, **2**, (see Figure 20b) at a MAS frequency of 30 kHz. BABA recoupling sequences of duration (a) two or (c) three τ_R were used for the excitation and reconversion of DQCs. The corresponding best-fit simulated three-spin ^{1}H DQ MAS spinning-sideband patterns are presented in (b) and (d). (Reproduced with permission from ref 30. Copyright 2001 American Chemical Society.)

is strong evidence that the intramolecular hydrogen-bonding arrangement shown in Figure 19 persists. On this basis and considering the intensities of the respective DQ peaks, the SQ resonances at 9.1 and 13.9 ppm can be assigned to the pyrrole NH and carboxylic acid OH protons, respectively.

In Figure 21 a and c, ^{1}H (700.1 MHz) DQ MAS spinning-sideband patterns obtained for the lactam (at 10.8 ppm) NH resonances of bilirubin, with τ_{rcpl} equal to (a) two and (c) three rotor periods at a ν_R = 30 kHz are shown. In the rotor-synchronized ^{1}H DQ MAS spectrum in Figure 20b, in addition to the intense NH−NH DQ peaks, weaker DQ peaks due to DQCs involving the OH and aliphatic protons are observed. An inspection of the spectra in Figure 21 reveals the existence of spinning sidebands due to all these different DQCs; note that the DQ peak for the NH−NH pair is at the second-to-left position.

In ref 30, a protocol is presented whereby the dominant D, and hence the shortest proton−proton distance, can be determined by finding the best fit simulated three-spin spectra on the basis of a comparison of the extracted integrated experimental sideband intensities with those in the simulated spectra. In this way, the distance between the lactam and pyrrole NH protons in bilirubin is determined to be 0.186 ± 0.002 nm (corresponding to a dominant D of 18.5 ± 0.5 kHz), proving an exceptionally close approach of two protons being noncovalently bonded to the same atom. The accuracy is better than what can be reliably expected from a standard X-ray structural analysis. We note that, at this degree of accuracy, the different effects of vibrational averaging should be considered, when comparing distances extracted by solid-state NMR to those determined by neutron diffraction studies.[136,158] The corresponding best-fit simulated three-spin spinning-sideband patterns are shown in Figure 21b,d. The analysis also yields a distance between the lactam NH and carboxylic acid OH protons of 0.230 ± 0.008 nm (corresponding to a perturbing D of 9.9 ± 1.0 kHz) and an H−H−H angle of 122 ± 4°—note that the precision of these values is less than for the case of the shortest proton−proton distance.

VII. Aromatic π–π Interactions and Ring-Current Effects

In addition to hydrogen-bonding effects, the ^{1}H chemical shift is very sensitive to the ring currents associated with aromatic moieties.[159] In comparison to the solution state, where isotropic molecular tumbling means that such effects are only seen for unusual intramolecular geometries,[160] in the solid state, the protons are exposed to the ring currents due to other nearby through-space aromatic moieties, be they intra- or intermolecular. However, it is only with the renewed interest in methods offering high resolution ^{1}H solid-state spectra that the widespread importance of ring current effects in the solid-state is being appreciated. It should be noted that ring current effects are not restricted to ^{1}H NMR—it will be shown below that shifts of the order of 1 ppm are also observed in the ^{13}C dimension. However, the effects are much more pronounced in ^{1}H NMR on account of the small chemical shift range and the usual location of the protons in "exposed" parts of the molecule.

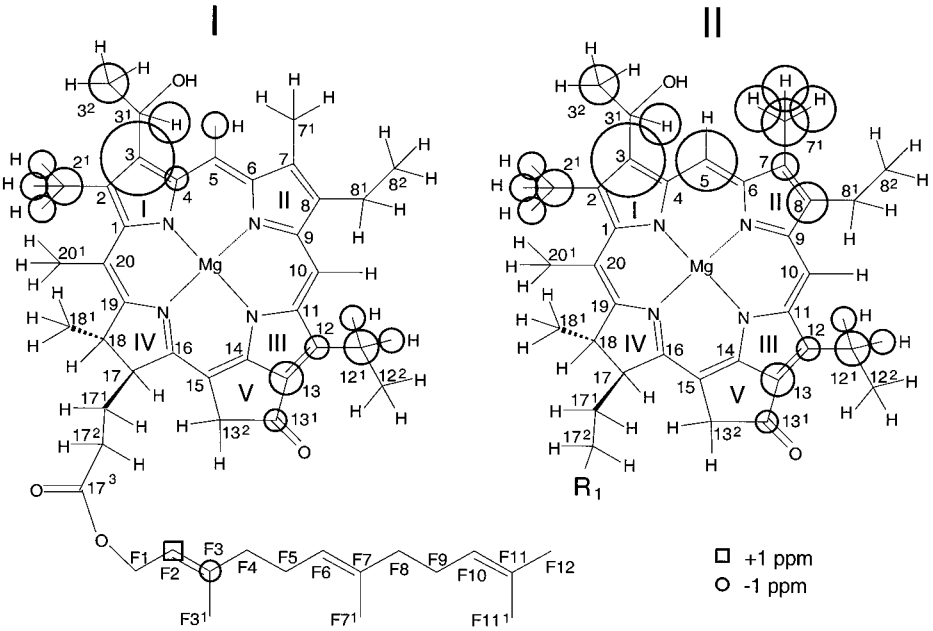

Figure 22. A representation of the aggregation shifts, i.e., the difference between the chemical shift in the aggregate (i.e., the solid state) and in the monomer (i.e., in solution), as determined for the ^{1}H and ^{13}C nuclei in a uniformly ^{13}C enriched bacteriochlorophyll (BChl) *c* in intact chlorosomes of *Chlorobium tepidum*, using 2D ^{1}H-^{13}C and 3D ^{1}H-^{13}C-^{13}C dipolar correlation spectroscopy at a magnetic field of 14.1 T. Circles correspond to upfield changes upon aggregation with the size of the circle indicating the magnitude of the change. The different representations in I and II correspond to the experimental observation of two separate components. (Reproduced with permission from ref 162. Copyright 2001 American Chemical Society.)

A. Aggregation Shifts

Probably the first clear example of the importance of ring current effects in ^{1}H solid-state NMR was presented by van Rossum et al.,[161] who were able to determine and assign the ^{1}H and ^{13}C chemical shifts in a uniformly ^{13}C enriched bacteriochlorophyll (BChl) *c* in intact chlorosomes of *Chlorobium tepidum*, using 2D ^{1}H-^{13}C and 3D ^{1}H-^{13}C-^{13}C dipolar correlation spectroscopy at a magnetic field of 14.1 T. As shown in Figure 22, what the authors refer to as "aggregation shifts", which are defined as the difference between the chemical shift in the aggregate (i.e., the solid state) and in the monomer (i.e., in solution), are observed for particular ^{1}H and ^{13}C nuclei. Note that in Figure 22, circles correspond to upfield changes upon aggregation with the size of the circle indicating the magnitude of the change. Making the assumption that these aggregation shifts are predominantly due to the ring currents arising from the aromatic moieties of nearby through-space molecules, the authors proposed a stacking arrangement that ensures overlap between only those aromatic moieties where the aggregation shifts are observed. Moreover, by combining the information provided by the NMR spectra with the results of modeling studies and electron microscopy, it was possible to propose a novel 3D suprastructure, namely, a bilayer tube, for the chlorosome antenna, which is of much interest on account of its role as a supramolecular light harvesting device.[162]

B. Hexabenzocoronone Derivatives

A striking example of the importance of ring-current effects in solid-state ^{1}H NMR is provided by the polycyclic aromatic molecule,[163] hexa-*n*-dodecyl-hexa-*peri*-hexabenzocoronene (henceforth referred to as HBC−C_{12}), **3**.[22] Note that, in the following, spectra

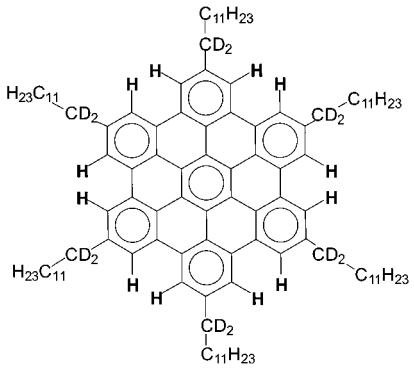

3

are presented for a sample in which the α-carbons of the alkyl side chains were deuterated (87%), this sample having been synthesized to carry out ^{2}H NMR. Figure 23a presents ^{1}H (500.1 MHz) MAS spectra of the solid phase of **3**, recorded at a ν_R of 35 kHz. The 6-fold symmetry of the individual molecules means that only one distinct aromatic proton resonance is expected, as is indeed found to be the case in the solution-state spectrum (not shown). However, in Figure 23a, three aromatic resonances are clearly identified.

In principle, the observed ^{1}H MAS spectrum in Figure 23a can be ascribed to two different scenarios: either there exist three different types of HBC crystallographic environment, where the 6-fold symmetry of each individual molecule is maintained, with the three environments then becoming equivalent in the LC phase, or there is a reduction of the 6-fold

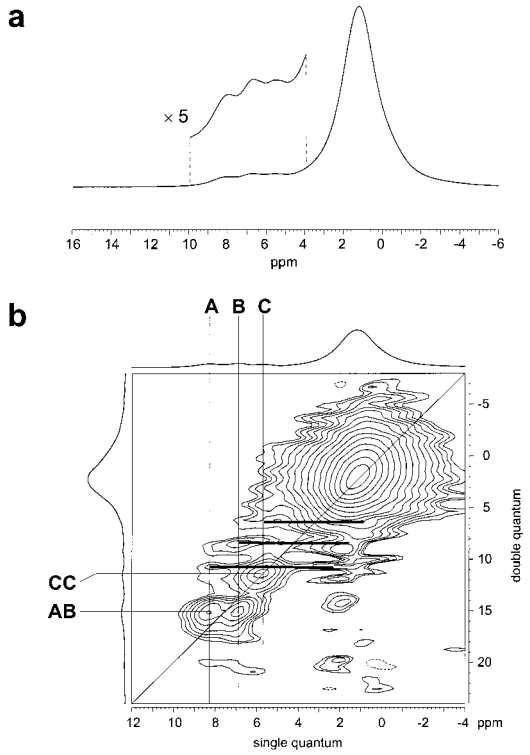

Figure 23. (a) ^{1}H (500.1 MHz) MAS (ν_R = 35 kHz) spectrum and (b) rotor-synchronized ^{1}H DQ MAS NMR spectrum, together with skyline SQ and DQ projections, of HBC−C_{12}, **3**. (Reproduced with permission from ref 22. Copyright 1999 American Chemical Society.)

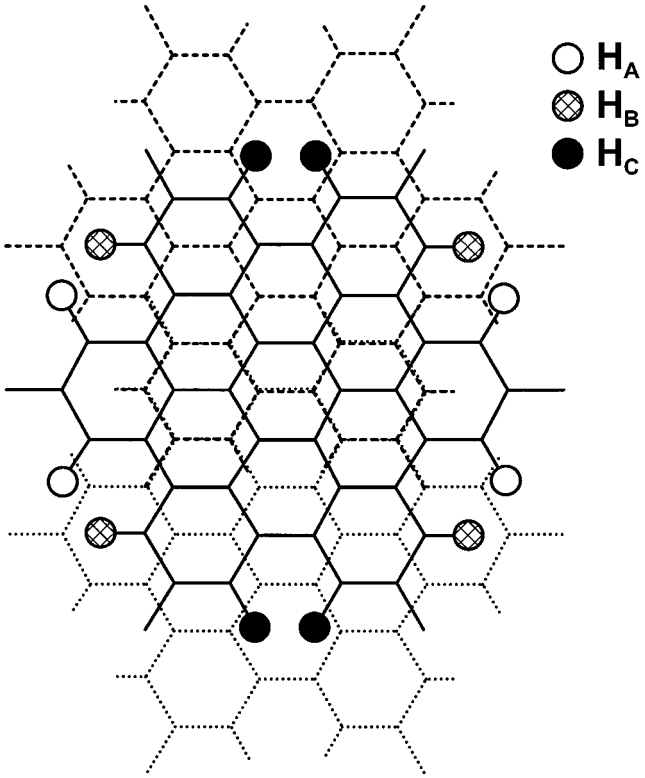

Figure 24. A representation of the proposed stacking of the aromatic cores in HBC−C_{12}, based on the structure of unsubstituted HBC, which is known, from a X-ray single-crystal study,[164] to crystallize in the so-called herringbone pattern. Three HBC−C_{12} molecules are shown; the molecules above and below the central HBC−C_{12} molecule are indicated by dashed and dotted lines, respectively. (Reproduced with permission from ref 22. Copyright 1999 American Chemical Society.)

symmetry of each molecule due to the packing arrangement in the crystal, leading to inequivalent aromatic proton sites within each HBC disk. These scenarios can be distinguished by DQ MAS NMR.

Information about the relative proximities of the three resolved aromatic protons is provided by the rotor-synchronized ^{1}H DQ MAS 2D spectrum of α-deuterated HBC−C_{12} in Figure 23b. Here, we focus on the peaks in the bottom left-hand corner of the spectrum, due to DQCs involving only aromatic protons—this spectral region is actually that which was shown in Figure 8a. As is evident from the molecular structure of HBC−C_{12}, the 12 aromatic protons are grouped in pairs of "bay protons" with a H−H distance of approximately 0.20 nm, while the closest distance to another aromatic proton is 0.41 nm. Therefore, the aromatic region of the DQ MAS spectrum will be dominated, for the short excitation period used here, by the dipole−dipole couplings within the three pairs. In Figure 23b, it is apparent that the extension to a second frequency dimension has yielded a significant resolution improvement over the one-dimensional spectrum (Figure 23a), and three separate resonances can be clearly distinguished. Strong CC auto and AB cross-peaks are observed, which imply the presence of only two types of pairs of aromatic protons, H_A-H_B and H_C-H_C, in a ratio, as determined from the peak intensities, of 2:1.

For unsubstituted HBC, an X-ray single-crystal study[164] showed that the molecules pack in the so-called herringbone pattern, which optimizes the $\pi-\pi$ interactions between adjacent disks. In ref 22, it was hypothesized that HBC−C_{12} adopts the same columnar packing of the aromatic cores as in unsubstituted HBC, with the presence of the long alkyl chains now meaning that the individual columns of aromatic cores are much more separated from each other. Figure 24 shows qualitatively how such a stacking of the HBC cores leads to three different aromatic proton environments. Three aromatic cores are shown; the molecules above and below the central aromatic core are indicated by dashed and dotted lines, respectively, with the aromatic protons of the central layer highlighted.

The interplanar distance in unsubstituted HBC is 0.342 nm,[164] and thus the aromatic protons of one layer will experience the ring currents of the extended π-electron systems of adjacent layers. In HBC−C_{12}, three different aromatic proton environments can thus be identified with respect to the degree to which the proton experiences the ring current of the adjacent layers. The unshaded circles represent protons that lie neither above nor below the π orbitals of an adjacent layer, and therefore correspond to the least shielded resonance (highest ppm). Fully shaded and hatched circles then represent protons that lie over or below an inner and outer part, respectively, of an adjacent ring system; the fully shaded protons would be expected to be the most shielded. Assigning the unshaded, hatched, and fully shaded protons to the A, B, and C resonances in Figure 23b, respectively, the observed presence of

only AB and CC pairs in the ratio 2:1, with the C resonance having the smallest chemical shift value (most shielded), is then explained. Thus, it is the second of the two scenarios, i.e., the reduction of the 6-fold to a 2-fold symmetry for each individual molecule, identified above which is borne out by experiment.

The advances in computing power as well as the development of methodology means that the use of quantum chemical calculations of NMR parameters in the interpretation of experimental results is becoming ever more popular.[165−167] As an example of the utility of such a combined experimental and theoretical approach, it has recently been shown that the ab initio calculation of ^{1}H chemical shifts for model HBC oligomers allows the quantitative assignment of the experimental observation of three aromatic resonances in HBC−C_{12} (see Figure 23) to a specific packing arrangement, with the qualitative hypothesis of the adoption of the structure of unsubstituted HBC (see Figure 24) being proved.[168] Moreover, these calculations showed that the ring currents effects are quite long-range, with an aromatic ring still exerting an influence at a distance of 0.7 nm, i.e., the next nearest HBC neighbor must be considered. We note that the further use of rotor-synchronized ^{1}H DQ MAS spectroscopy and ab initio quantum chemical calculations to investigate two other HBC derivatives is described in refs 24 and 169.

C. A Molecular Tweezer Host–Guest Complex

As the final example in this section, we show how an investigation of the changes in ^{1}H chemical shifts caused by aromatic ring currents provides insight into the nature of the supramolecular host−guest complex, **4**@**5**.[29] The receptor **4** belongs to a family

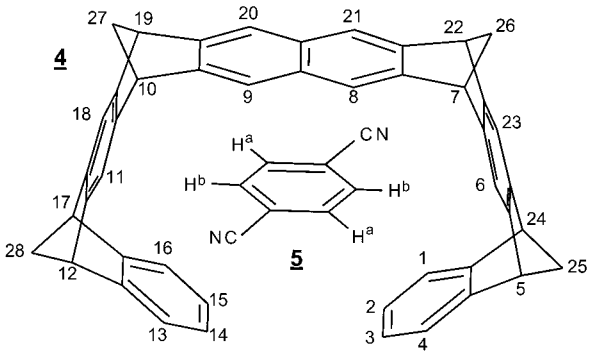

of molecules termed molecular tweezers due to their concave−convex topology and propensity to selectively form complexes with electron-deficient aromatic and aliphatic compounds as well as organic cations.[170,171] This and other molecular tweezer host−guest complexes have been studied by ^{1}H solution-state NMR, exploiting the large upfield shifts of the substrate resonances upon complexation caused by host aromatic ring currents. For the specific complex studied here between the naphthalene-spaced tweezer **4** and 1,4-dicyanobenzene **5**, complex formation and dissociation in $CDCl_3$ at room temperature is fast with respect to the NMR time scale, as evidenced by a single guest ^{1}H resonance shifted by 4.35 ppm

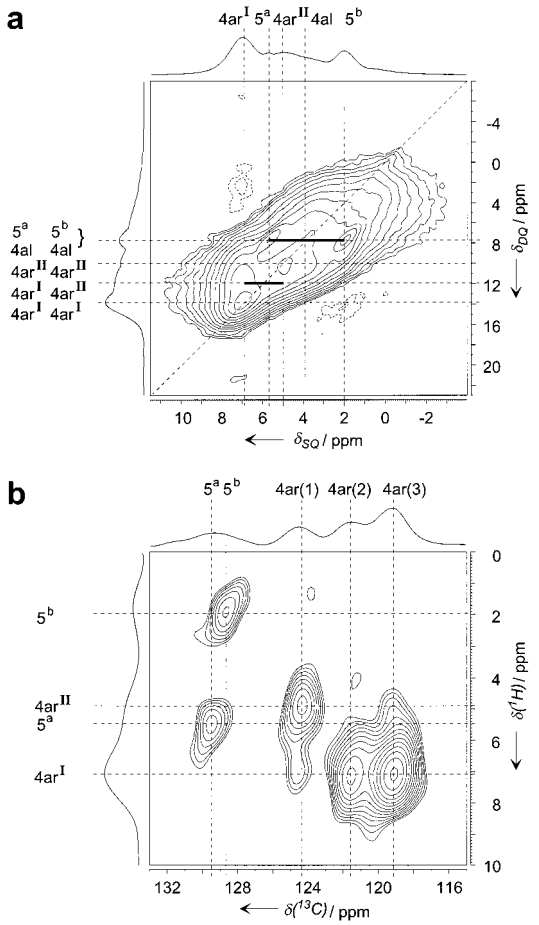

Figure 25. (a) Rotor-synchronized ^{1}H(700.1 MHz) DQ MAS NMR spectrum, together with skyline projections, of **4**@**5**. (b) The aromatic region of a ^{1}H-^{13}C REPT-HSQC NMR correlation spectrum, together with sum projections, of **4**@**5**. Both spectra were recorded under MAS at 30 kHz. The recoupling time equalled one rotor period, such that predominantly only one-bond correlations are selected. The notations **4**ar and **4**al refer to host aromatic and alkyl protons, respectively, while $\mathbf{5}^a$ and $\mathbf{5}^b$ refer to the two distinct guest aromatic protons. (Reproduced with permission from ref 29. Copyright 2001 Wiley.)

relative to that observed for **5** alone. A solid-state investigation has the advantage that the guest remains complexed on the time scale of the NMR experiment, and thus the structure and dynamics of the host−guest complex can be probed directly. It should be noted that an X-ray single-crystal structure is available for **4**@**5**;[171] therefore, this study offers the opportunity to check the reliability of the described approach and to demonstrate that additional complementary insight can be provided.

Figure 25a presents a rotor-synchronized ^{1}H (700 MHz) DQ MAS NMR spectrum of **4**@**5**. The assignment of the resolved ^{1}H DQ peaks is aided by reference to Figure 25b, where the aromatic region of a ^{1}H-^{13}C heteronuclear correlation spectrum of **4**@**5**, recorded with the REPT-HSQC experiment shown in Figure 13, is presented. A short excitation time was used such that predominantly only one-bond C−H correlations are observed. In solution, the aromatic CH resonances of **4** and **5** are found between 116.5 and 124.1 and at 131.0 ppm, respectively. The relative insensitivity of ^{13}C chemical shifts to ring

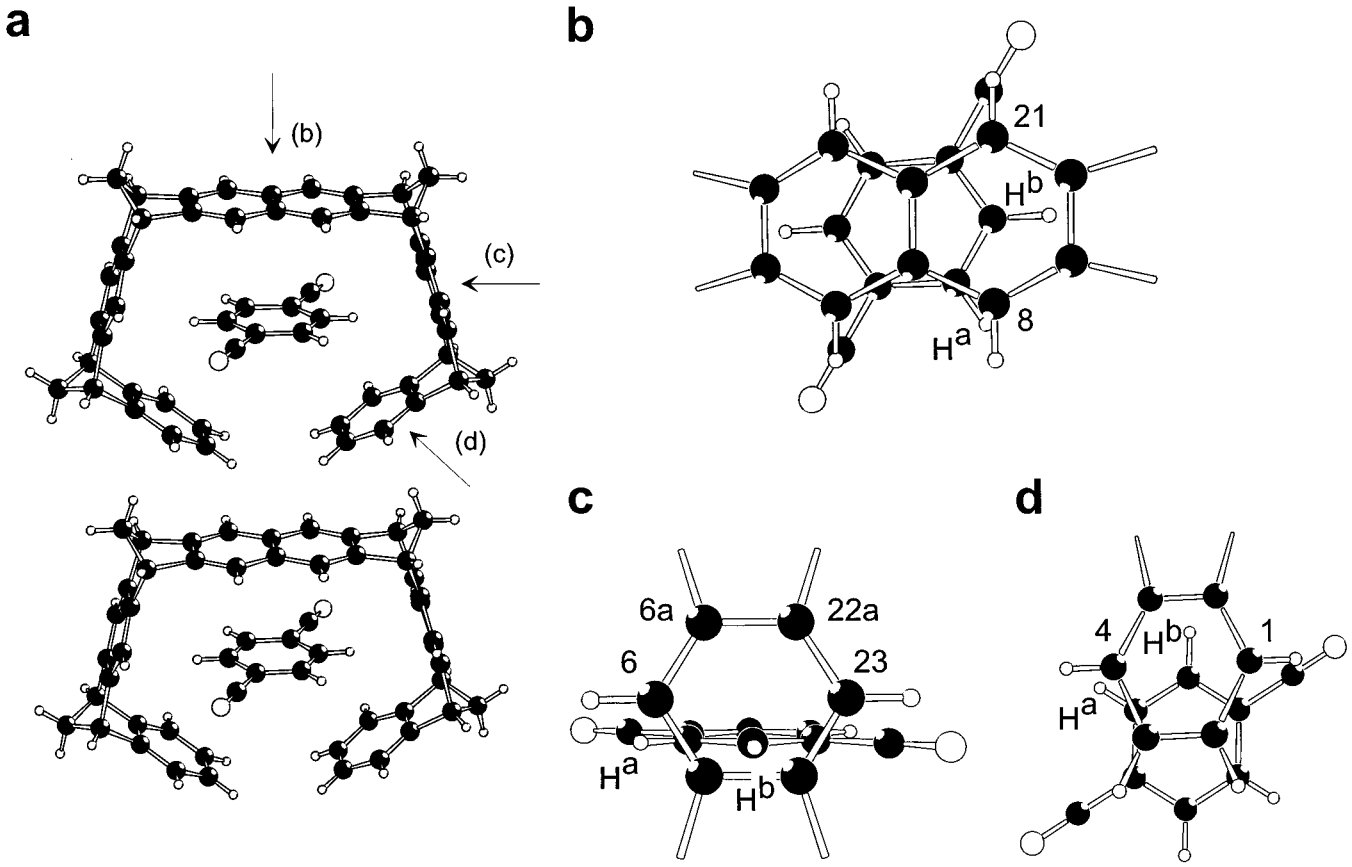

Figure 26. The solid-state packing arrangement of **4**@**5**, as determined by an X-ray single-crystal investigation.[171] Large white, large black, and small white circles represent nitrogen, carbon, and hydrogen atoms, respectively. In (b), (c) and (d), views through the naphthalene, inner benzene and outer benzene rings, respectively, are shown. The distance from H^b to the center of the inner benzene ring is 260 pm (view (c)) as opposed to 404 pm to the middle of the naphthalene unit (view (b)) and 314 pm to the center of the outer benzene ring (view (d)). Specific carbon and hydrogen atoms are labeled according to the above chemical structure. (The notation xa refers to the quaternary carbon between carbons x and x+1.) (Reproduced with permission from ref 29. Copyright 2001 Wiley.)

current effects then allows the clear assignment of the two separate peaks at ^{13}C chemical shifts of 129.6 and 128.7 ppm in Figure 25b to the guest CHs (labeled **5**a and **5**b), with the corresponding ^1H chemical shifts being 5.6 and 2.0 ppm, respectively.

The pair of cross-peaks at a DQ frequency of 7.6 ppm in Figure 25a can thus be identified as being due to two neighboring guest CH protons. It is further interesting to note that two distinct host aromatic ^1H resonances can be resolved in both the ^1H DQ MAS and ^1H-^{13}C REPT-HSQC spectra: the ^{13}C peak at 124.4 ppm (**4**ar(1)) can be assigned to the meta pair of carbons of the outer benzene ring (2, 3, 14, and 15), with the corresponding ^1H chemical shift being 4.9 ppm (**4**ar^{II}). From Figure 25b, the other aromatic protons have, within the experimental resolution, the same chemical shift of 7.1 ppm (**4**ar^{I}). In this way, the observation of diagonal ^1H DQ peaks at 13.8 and 10.0 ppm, as well as shoulders corresponding to DQ cross-peaks at 12.0 ppm can be explained.

The observed experimental features can be qualitatively understood by reference to the structure of **4**@**5**, which is known from an X-ray single-crystal analysis.[171] In Figure 26a, the side-by-side arrangement of two **4**@**5** complexes is displayed, while Figures 26b, 26c, and 26d show views through the different host aromatic moieties. It is apparent that the two guest aromatic protons experience the ring currents due to the host to different degrees. Moreover, from Figure 26a, the end pair of aromatic protons can be seen to be directed into the ring current due to the naphthalene unit of the next host, explaining the **4**ar^{II} resonance.

As was the case with the HBC−C_{12} example discussed above, ab initio quantum chemical calculations were carried out, thus providing a fully quantitative interpretation of the experimental results. Table 2 presents the experimental solution- and solid-state ^1H chemical shifts obtained by quantum chemical calculations (for details, see ref 29) for a single

Table 2. Comparison of the ^1H Chemical Shifts (in ppm) for 4@5 Determined by NMR Experiments and ab Initio Calculations[29]

	solution-state NMR	solid-state NMR	ab initio (monomer)	ab initio (dimer)
H^a (guest)	3.5	5.6	5.5	5.2
H^b (guest)	3.5	2.0	2.5	2.1
H2,3,14,15	6.4	4.9	6.6	5.5−5.6
other arom	7.0−7.2	7.1−7.2	7.2−8.0	6.9−7.7
$H_{bridgehead}$	4.1	3.8[a]	3.9−4.2	3.3−4.0
H25,28[b]	2.4	2.0−3.8[a]	2.2	2.1
H26,27[b]	2.5	0.6−2.3[a]	2.0−2.1	0.4−1.0

[a] These ^1H chemical shifts were determined from the alkyl region of the ^1H-^{13}C correlation spectrum (not shown). [b] Note that the two protons in each CH_2 group are inequivalent.

4@**5** complex and a pair of **4**@**5** complexes in the arrangement shown in Figure 26a (denoted as monomer and dimer, respectively). The good agreement between the monomer calculation and the experimental solid-state *guest* ^{1}H chemical shifts reveals that these values are largely determined by *intra*-complex effects. In contrast, the marked difference between the solid- and solution-state ^{1}H chemical shifts of the end pair of host aromatic protons (H2,3,14,15) can only be explained by considering a *dimer*.

By calculating the ^{1}H chemical shifts of the guest protons due to the three host aromatic moieties, namely, the central naphthalene unit (Figure 26b), and the inner (Figure 26c) and outer benzene ring (Figure 26d), the quantum chemical calculations were further able to elucidate the role of the different chemical units. First, it was found that the guest ^{1}H chemical shifts derived by summing the changes due to the separate aromatic moieties are in good agreement with the values calculated for the whole system. It can thus be concluded that the only influence of the linking units is to determine the positioning of the host aromatic moieties. Second, the difference between the guest ^{1}H chemical shifts is mainly due to the arrangement of the guest with respect to the inner benzene ring (Figure 26c).

VIII. The Investigation of Dynamic Processes

A unique strength of solid-state NMR is its ability to probe molecular dynamics with site selectivity.[9,132] In this section, we present some specific examples that illustrate the considerable insight into dynamic processes provided by advanced solid-state NMR experiments applicable to as-synthesized samples, i.e., without the requirement for isotopic labeling. These examples focus on well-defined processes that are fast as compared to the time scale of the ^{1}H DQ MAS experiment, this being on the order of 10^{-6} to 10^{-4} s. In addition, it should be noted that the extraction of dipolar couplings by following the build-up of DQC in a ^{1}H DQ MAS experiment has been shown to provide insight into the complex dynamic processes in polymer melts,[172] block copolymers,[173] and elastomers.[174]

A. A Molecular Tweezer Host–Guest Complex

Figure 27 presents slices at a DQ frequency of 7.6 ppm taken from ^{1}H DQ MAS spectra of **4**@**5** (discussed in section VII C) recorded at different temperatures.[29] It is to be noted that the heating due to friction at a very-fast ν_R is significant, and in the examples presented in this section, the correction term relative to the bearing gas temperature was calibrated using the ^{119}Sn resonance of $Sm_2Sn_2O_7$ as a chemical shift thermometer.[175] The peaks due to the guest protons, H^a (5.6 ppm) and H^b (2.0 ppm), disappear upon heating, indicating dynamic processes, (see Figure 27) where the two types of guest protons are exchanged by either (A) a 180° flip about the long axis of the guest, or (B) a rotation between two equivalent sites in the complex. A quantitative analysis is hampered by the peak at 3.9 ppm due to host alkyl protons—the fast exchange peak would be expected to appear at exactly this position. It was noted, though, that no peak was observed in a slice corresponding to the guest ^{13}C CH resonance in a ^{1}H-^{13}C correlation spectrum recorded at 410 K (spectrum not shown). Thus, it can be concluded that, at this temperature, the exchange process is in the intermediate regime, i.e., coalescence. From the difference in the chemical shifts of the guest protons H^a and H^b ($\Delta\delta = 3.8$ ppm), the rate constant for the exchange process at 410 K can be estimated to be 5600 s^{-1}, corresponding to a Gibbs free enthalpy of activation, $\Delta G^{\ddagger}$, of 72 kJ mol^{-1}.[176]

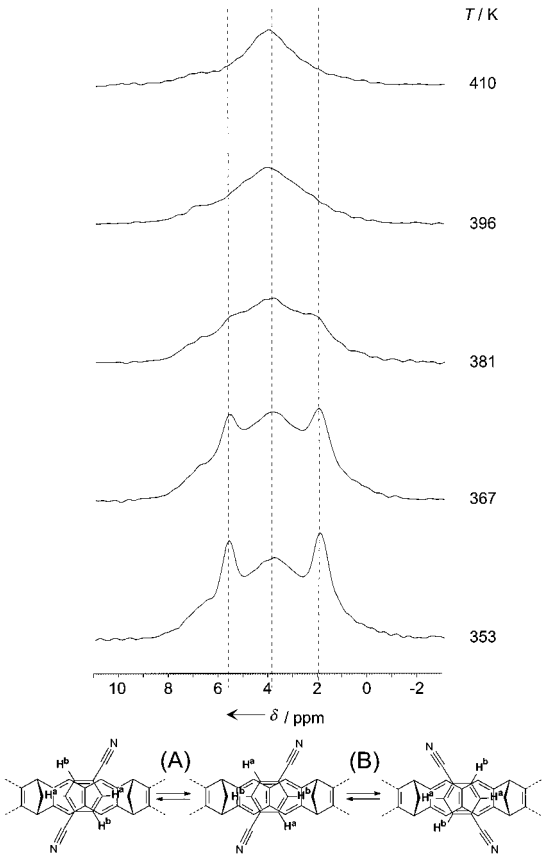

Figure 27. The effect of temperature, *T*, on slices at a DQ frequency of 7.6 ppm taken from ^{1}H (700.1 MHz) DQ MAS NMR spectra of **4**@**5**. At the bottom, the dynamic processes consistent with the observed NMR results are shown. The two processes, (A) and (B), cannot be distinguished by current NMR experiments. (Reproduced with permission from ref 29. Copyright 2001 Wiley.)

B. The Making and Breaking of Hydrogen Bonds in a HBC Derivative

The established importance of hydrogen bonds in biological systems as well as the recognized potential for their incorporation into synthetic systems lies in the relative ease with which they can be broken and then reformed. It is thus essential that methods exist by which hydrogen bond dynamics can be investigated. Using ^{2}H solid-state NMR, hydrogen exchange by proton tunneling between the two tautomeric forms of a carboxylic acid dimer has been probed,[177] while intramolecular hydrogen-bond exchange dynamics have been extensively investigated by Limbach and co-workers using ^{15}N solid-state NMR, e.g.,

in *N*,*N*-bisarylformamidines[178] or a phenylenediamine.[179] In this subsection, we will show that the resolution routinely achievable in ^{1}H solid-state NMR methods allows the making and breaking of hydrogen bonds to be directly probed.

Consider the hexabenzocoronene (HBC) derivative, 2, 5, 8, 11, 14, 17-hexa[10-carboxydecyl]hexa-*peri*-hexabenzocoronene, **6**, (henceforth referred to as

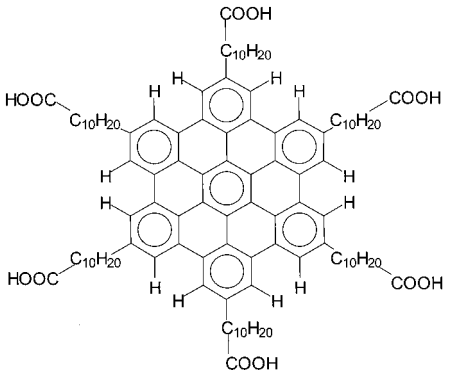

6

HBC−C_{10}COOH), where all six alkyl chains have been capped by a carboxylic acid group.[25] In the solid phase at $T = 320$ K, the presence of hydrogen-bonded COOH dimers is demonstrated by the observation of an auto COOH peak in the ^{1}H DQ MAS NMR two-dimensional spectrum; see Figure 28. Considering the COOH peak in the one-dimensional ^{1}H MAS spectra, as shown in Figure 29a, both a shift to high field of the peak position as well as an initial increase followed by a subsequent decrease in the line width are observed upon heating. These effects are represented graphically in Figure 30a,b. These observations are interpreted in terms of a chemical exchange process involving the making and breaking of hydrogen bonds, with the coalescence point corresponding to $T = 362$ K.

The equilibrium constant at a given temperature can be calculated from the observed chemical shift

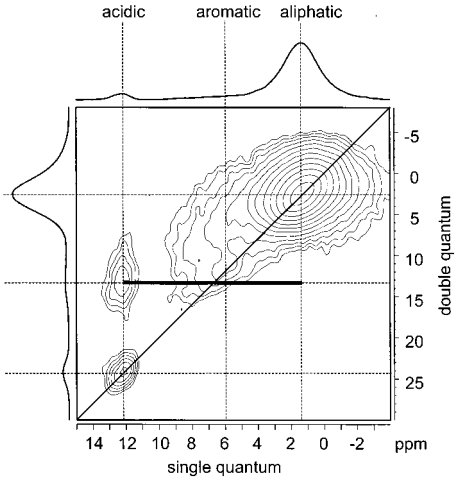

Figure 28. Rotor-synchronized ^{1}H (500.1 MHz) DQ MAS ($\nu_R = 30$ kHz) NMR spectrum, together with skyline SQ and DQ projections, of the room-temperature phase of as-synthesized HBC−C_{10}COOH, **6**. (Reproduced with permission from ref 25. Copyright 2000 The PCCP Owner Societies.)

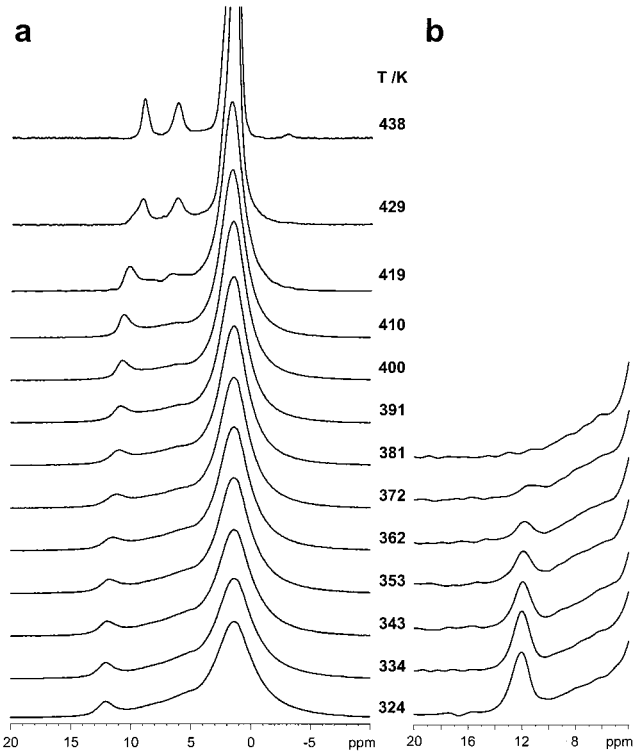

Figure 29. The effect of temperature on (a) ^{1}H (500.1 MHz) MAS ($\nu_R = 30$ kHz) and (b) ^{1}H DQF MAS NMR spectra of as-synthesized HBC−C_{10}COOH, **6**. (Reproduced with permission from ref 25. Copyright 2000 The PCCP Owner Societies.)

provided that the ^{1}H chemical shifts of the hydrogen-bonded and free states are known. Only the COOH protons in hydrogen-bonded dimers can give rise to a COOH auto peak in the ^{1}H DQ MAS spectrum (Figure 28), and thus the chemical shift of the hydrogen-bonded protons can be determined to be 12.1 ppm. The chemical shift of the free COOH protons cannot be so easily identified; however, the initially observed chemical shift of 9.0 ppm for the COOH protons on heating into the LC phase is strikingly low, and it is thus assumed that the chemical shift of the free state can be assigned to this value. A thermodynamic analysis yields for the opening of the hydrogen-bonded dimers: $\Delta H = 45 \pm 4$ kJ mol^{-1} and $\Delta S = 113 \pm 11$ J K^{-1} mol^{-1}.

In ^{1}H DQ-filtered (DQF) MAS spectra of HBC−C_{10}COOH (see Figure 29b), the intensity of the COOH peak is observed, upon heating, to reduce faster than expected from thermodynamic factors alone, and above $T = 380$ K, no signal is detected, see Figure 30c, where the experimentally observed DQ signal intensities for the COOH protons, relative to the intensity of the $T = 324$ K spectrum, are shown as crosses, while circles represent the expected reduction, again relative to the $T = 324$ K case, due solely to the combined temperature dependence of the equilibrium constant and the bulk magnetization. At $T = 381$ K, where the COOH peak intensity disappears below the noise level in Figure 29b, the number of hydrogen-bonded and free COOH protons are known, on the basis of the thermodynamic analysis described above, to be in the ratio ~3:2; thus, the loss of signal cannot be due to the absence of pairs of COOH protons in close proximity.

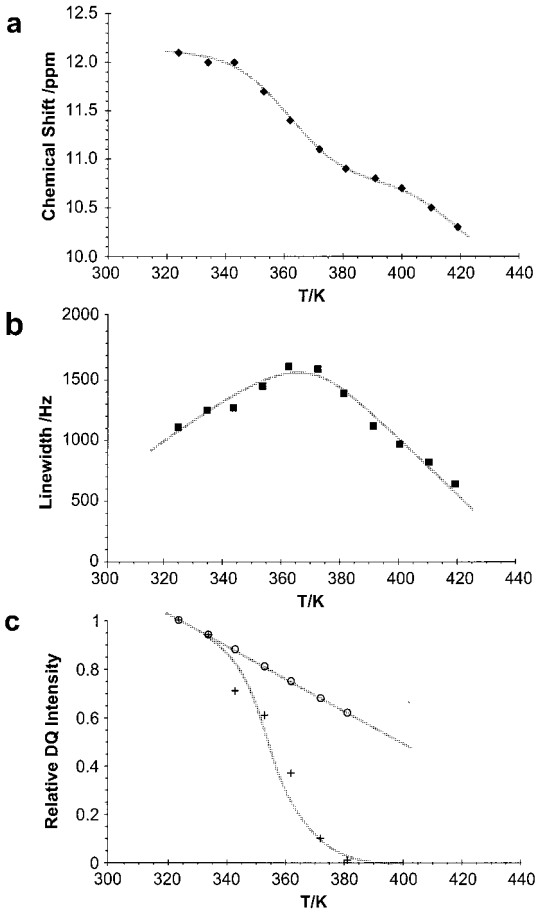

Figure 30. The effect of temperature on (a) the observed chemical shift and (b) the line width (fwhmh) in ^{1}H MAS spectra (Figure 28a), and (c) the intensity in ^{1}H DQF MAS spectra (Figure 28b) of the COOH resonance for a sample of as-synthesized HBC−C_{10}COOH, **6**. In (c), in addition to the crosses, which represent the experimental DQF intensities, the intensities that are expected on account of solely the combined temperature dependence of the equilibrium constant and the NMR bulk magnetization are shown as circles. Both the experimental and thermodynamically expected intensities are normalized relative to the $T = 324$ K case. In all plots, best-fit lines are included as a guide for the eye. (Reproduced with permission from ref 25. Copyright 2000 The PCCP Owner Societies.)

To observe a signal in a DQF experiment, the hydrogen-bonded form must exist for the duration of the DQ filter part of the NMR experiment, i.e., 133 μs for the spectra in Figure 29b. It is then apparent that the fall off in the DQ intensity with increasing temperature can be explained by a decrease in the proportion of hydrogen-bonded dimers having lifetimes over 133 μs, until at $T = 381$ K, the concentration is less than that required to observe an NMR signal. In this way, an analysis of the DQF data yields the temperature dependence of the dimer lifetimes, and hence the kinetics of the exchange process could be determined: the activation energy and Arrhenius parameter equal 89 ± 10 kJ mol^{-1} and 4.2×10^{16} s^{-1}, respectively.

C. The Order Parameter in Columnar Discotic Mesophases

The HBC derivatives introduced in the previous sections represent a relatively new family of discotic aromatic mesogen, which have a number of favorable properties as compared to the more established triphenylenes; for example, the mesophases are stable over a very wide temperature range[180] and exhibit an exceptionally high one-dimensional charge carrier mobility.[181] In this section, we will show that the recording of homo- and heteronuclear MQ spinning-sideband patterns allows the order parameter of the LC phases to be quantitatively determined.

Figure 31 presents experimental ^{1}H DQ MAS spinning sideband patterns for the aromatic protons in (a) the crystalline and (b) the LC phases of α-deuterated HBC−C_{12}.[22] The MAS frequency was 35 and 10 kHz in (a) and (b), respectively, with two rotor periods being used for excitation/reconversion in both cases, such that τ_{rcpl} equals 57 and 200 μs in the two cases. The dotted lines represent best fit spectra simulated using the analytical time-domain expression for an isolated spin pair in eq 6. As noted in section VIIB, the aromatic protons exist as well isolated pairs of bay protons, and, thus, an analysis based on the spin-pair approximation is appropriate here. As is evident from the insets on the right of Figure 31, the DQ MAS spinning sideband patterns are very sensitive to the product of the D and τ_{rcpl}. The best-fit spectra for the solid and LC phases then correspond to $D/(2\pi)$s equal to 15.0 ± 0.9 and 6.0 ± 0.5 kHz, respectively.

Comparing the evaluated D values for the crystalline and LC phases, a reduction of D by a factor of 0.40 ± 0.04 is observed, corresponding to an order parameter[182] of 0.80 ± 0.08. In the LC phase, fast axial rotation of the molecule about an axis perpendicular to the ring (passing through the center of symmetry) is expected.[182] For a molecule undergoing such a motion, the dipolar coupling constant is reduced by a factor of $1/2(1 - 3\cos^2\theta)$, where θ is the angle between the principal axes system (here the internuclear vector) and the molecular rotation axis.[183] (Note that this dynamic averaging term is not included in the earlier definition of D in eq 1.) Thus, for the case where the internuclear vector is perpendicular to the rotation axis ($\theta = 90°$), a reduction by a factor of 0.5 is expected. The value of 0.40 can be explained by postulating the presence of out-of-plane motion in addition to the axial rotation. The ability to probe such motion is of much importance, since it is likely to impair efficient charge carrier mobility.

As a complementary alternative to using the change in a H−H dipolar coupling to probe a dynamic process, methods that determine heteronuclear ^{1}H-^{13}C dipolar couplings offer much promise. Figure 32 presents, on the left-hand side, ^{1}H-^{13}C spinning-sideband patterns obtained at the aromatic C−H ^{13}C resonance for the solid and LC phases of HBC−C_{12}, using the REPT-HMQC experiment discussed in section IVB.[37] In addition, the dotted lines represent simulated spectra, obtained using the best-fit D for the CH groups, namely, 20.9 ± 0.5 and 8.2 ± 0.9 kHz for the solid and LC phases, respectively. The order parameter is hence determined to be 0.78 ± 0.09. This value, thus, agrees with that determined from the analysis of ^{1}H DQ MAS spinning-sideband patterns discussed above. In addition, these values are

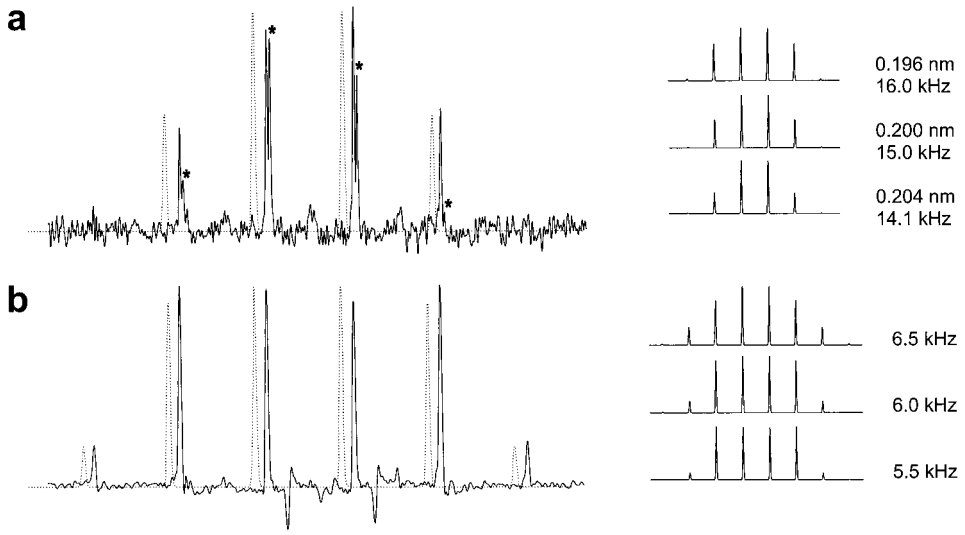

Figure 31. Extracted columns from ^{1}H (500.1 MHz) DQ MAS spectra of HBC−C_{12}, **3**, showing the DQ spinning sideband patterns for (a) the aromatic protons at 8.3 ppm in the solid phase (T = 333 K), and (b) the aromatic protons at 6.2 ppm in the LC phase (T = 386 K). In each case, best-fit spectra, generated according to the spin-pair expression in eq 6, are shown (shifted to the left to allow a better comparison) as dotted lines. A spinning frequency, ν_R, equal to 35 and 10 kHz was used for the solid and LC phases, respectively, with the two rotor-period compensated BABA recoupling sequence being used for the excitation and reconversion of DQCs in both cases. In (a), additional peaks corresponding to DQCs between aromatic and residual undeuterated α-carbon protons are marked by *. The insets to the right of the experimental spectra show the sensitivity of the spinning-sideband patterns to the product $D\tau_{rcpl}$. (Reproduced with permission from ref 22. Copyright 1999 American Chemical Society.)

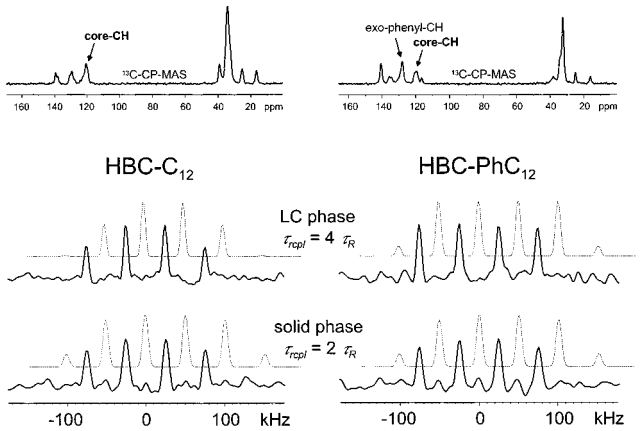

Figure 32. ^{1}H-^{13}C heteronuclear MQ MAS spinning-sideband patterns, obtained at a ν_R = 25 kHz, using the REPT-HMQC experiment. The patterns correspond to the sum projections over the ^{13}C resonance due to the aromatic core CH in the 2D spectra of HBC−C_{12}, **3**, and HBC−PhC_{12}, **7**. The spectra for the room temperature (solid) and high-temperature LC phases were recorded at 35 and 120 °C, respectively. The dotted traces represent simulated spectra, obtained by taking into account the best-fit Ds for the CH groups. At the top, ^{13}C CP-MAS (ν_R = 15 kHz) spectra are presented, with the signal positions of the aromatic CH resonances being identified. (Reproduced with permission from ref 37. Copyright 1999 Wiley.)

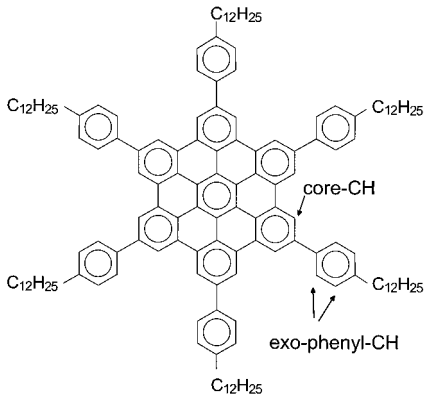

7

in agreement with a value of 0.84 obtained from an analysis of ^{2}H 1D NMR line shapes.[180]

An advantage of the heteronuclear ^{1}H-^{13}C approach is that it benefits from the better resolution in a ^{13}C SQ dimension. An example of this is provided by the hexa(*para-n*-dodecylphenyl)-substituted HBC (henceforth referred to as HBC−PhC_{12}), **7**.[37] In this case, ^{1}H solid-state NMR is unable to distinguish the core and exo-phenyl protons. By comparison, as shown in the ^{13}C CP MAS spectrum at the top right of Figure 32, the corresponding ^{13}C resonances are well resolved. It is thus possible to use the heteronuclear approach to probe separately the dynamics of the core and the outer phenyl rings. For example, the right-hand-side of Figure 32 presents ^{1}H-^{13}C spinning-sideband patterns obtained at the core aromatic CH ^{13}C resonance for the solid and LC phases of HBC−PhC_{12}, using the REPT-HMQC experiment.

A comparison of the spinning-sideband patterns obtained for the LC phases of HBC−C_{12} and HBC−PhC_{12} reveals that the third-order spinning sidebands are significantly higher in the latter case; they are of the same height as the first-order spinning sidebands for HBC−PhC_{12}. Since the same experimental conditions were used in both cases, this result immediately indicates a larger dipolar coupling and, hence, a larger order parameter for HBC−PhC_{12}. Indeed, the order parameter is determined to be 0.93 ± 0.09, indicating less out-of-plane mesogen mobility. It is interesting that this NMR result is correlated with an improved intra- and intercolumnar packing as evidenced by powder X-ray diffraction patterns.[37]

Finally, we note that an analysis of ^1H-^{13}C spinning-sideband patterns obtained using the REPT-HDOR experiment (see Figure 16) has also been used to provide evidence of restricted dynamics in a shape-persistent polyphenylene dendrimer.[184]

IX. Conclusions

In this review, we have demonstrated that the advanced solid-state NMR methods existing today are well placed to provide answers to the structural and dynamic questions of relevance in modern polymer chemistry. In particular, the further development of high-resolution ^1H solid-state NMR methods has opened up the possibility of routinely directly probing hydrogen-bonding and aromatic $\pi-\pi$ interactions. It is to be emphasized that only 10−20 mg of a powdered as-synthesized sample is required, i.e., there is no need for synthetically demanding selective isotopic labeling or a single crystal. Moreover, the potential applications of solid-state NMR are not restricted to the many examples given in the previous sections: in our laboratory, for example, preliminary results have been obtained that provide insight into proton conduction in imidazole-based materials as well as the local order and dynamics in the cylindrical macromolecules synthesized by Percec and co-workers, which were mentioned in the introduction.

Solid-state NMR spectroscopy should certainly not be used in isolation. For example, when a new sample is to be investigated, we insist, in our laboratory, on receiving assigned ^1H and ^{13}C solution-state NMR spectra (except, of course, for cases where the sample is insoluble). An example of the importance of this is provided by the ^1H-^{13}C correlation spectrum of the host−guest complex in Figure 25b, where the assignment of the guest resonances is based on the known solution-state ^{13}C chemical shifts and the comparative insensitivity of ^{13}C chemical shifts to through-space aromatic ring currents.

In addition, if dynamic processes are to be investigated, it is very useful if differential scanning calorometry (DSC) curves can be first obtained, so that the temperatures at which phase transitions occur are known in advance. Moreover, when carrying out variable temperature studies of organic solid, it is important to be aware of the fact that the observed behavior, in terms of, e.g., phase transition temperatures and NMR spectra, can differ significantly depending on whether the solid phase formed from solution or from a LC phase or melt. It is, therefore, necessary to see both the first and subsequent DSC heating curves; a clear example of this phenomenon is described in ref 25. Furthermore, we note that, in our experience, different batches of a material, synthesized by the same procedure, can give slightly different solid state ^1H NMR spectra, even though the purity of the material as determined by standard methods, e.g., solution-state NMR, is judged to be the same. This is particularly the case for hydrogen-bonded systems, and thus it seems that solid-state NMR is able to distinguish subtly different packing arrangements, suggesting potential quality-control applications.

As stated in section V, solid-state NMR should not be considered as a replacement for the established diffraction methods. Instead, the two methods should be thought of as being complementary, since they have much to offer each other. For example, as discussed in section VIIB, the existence of a single-crystal X-ray structure for unsubstituted HBC allowed a qualitative interpretation of the observed ^1H DQ MAS spectrum of HBC−C_{12}, where it was not possible to obtain a single-crystal suitable for an X-ray analysis. The symbiosis between ^1H solid-state NMR and X-ray single-crystal methods was further well illustrated by the case of bilirubin in section VIB, where an X-ray single-crystal structure exists. On one hand, the reliable establishing of the heteroatom positions facilitated the assignment of the observed peaks in the ^1H DQ MAS spectrum. On the other hand, it was shown that an analysis of ^1H DQ MAS spinning-sideband patterns allowed the determination of the distance between two hydrogen-bonded protons to a precision of $\pm$ 0.002 nm; since structure determination by single-crystal X-ray diffraction methods, being based on the diffraction of X-rays by electrons, is not well suited to the localization of lighter atoms, the ability of solid-state NMR to provide distance constraints, which can be used in the optimization of a crystal structure, in particular, the very relevant hydrogen-bonded part, is of much importance.

In section VII, the value of a combined experimental and theoretical approach, incorporating the ab initio calculation of ^1H chemical shifts, was illustrated. First, in section VIIB, it was stated that the calculation of ^1H chemical shifts for model HBC oligomers allowed the quantitative assignment of the experimental observation of three aromatic resonances in HBC−C_{12} to a specific packing arrangement. Moreover, in section VIIC, the ability to identify the importance of intra- and intercomplex interactions as well as the role of the separate aromatic moieties was discussed. The advances in computing power as well as the development of methodology means that the use of quantum chemical calculations of NMR parameters in the interpretation of experimental results will become ever more popular.

It should not be forgotten that the development of advanced solid-state NMR methodology is an area of ongoing active research. For example, as evidenced by section II, various groups are pursuing the goal of reducing the ^1H solid-state NMR line width ever further. Moreover, the utility of the ^1H DQ MAS method would be much enhanced if homonuclear decoupling methods, which, as illustrated by Figure 5, yield a striking improvement in the ^1H line width as compared to very-fast MAS, could be incorporated in a robust and artifact-free manner. It is to be hoped that the problems of significant spectral artifacts encountered in an earlier attempt to combine ^1H DQ MAS spectroscopy with the multiple-pulse assisted MAS approach[20] can be overcome. To conclude, it is envisaged that solid-state NMR can become as highly valuable to the chemist as solution-state NMR is today.

X. Acknowledgment

We thank Prof. Lyndon Emsley, Dr. Robert Graf, Dr. Kay Saalwächter, and Dr. Ingo Schnell for helpful comments on the manuscript. We are also very grateful to Prof. Huub de Groot and Prof. Lyndon Emsley for providing preprints of unpublished articles.

XI. References

(1) Prins, L. J.; Reinhoudt, D. N.; Timmerman, P. *Angew. Chem., Int. Ed. Engl.* **2001**, *40*, 2382.
(2) Sijbesma, R. P.; Beijer, F. H.; Brunsveld, L.; Folmer, B. J. B.; Hirschberg, J. H. K. K.; Lange, R. F. M.; Lowe, J. K. L.; Meijer, E. W. *Science* **1997**, *278*, 1601.
(3) Hudson, S. D.; Jung, H.-T.; Percec, V.; Cho, W.-D.; Johansson, G.; Ungar, G.; Balagurusamy, V. S. K. *Science* **1997**, *278*, 449.
(4) Percec, V.; Cho, W.-D.; Ungar, G. *J. Am. Chem. Soc.* **2000**, *122*, 10273.
(5) Ernst, R. R.; Bodenhausen, G.; Wokaun, A. *Principles of Nuclear Magnetic Resonance in One and Two Dimensions*; Clarendon: Oxford, 1987.
(6) Claridge, T. D. W. *High-Resolution NMR Techniques in Organic Chemistry*; Pergamon: Amsterdam, 1999.
(7) Sattler, M.; Schleucher, J.; Griesinger, C. *Prog. NMR Spectrosc.* **1999**, *34*, 93.
(8) Mehring, M. *Principles of High-Resolution NMR in Solids*; Springer: Berlin, 1983.
(9) Schmidt-Rohr, K.; Spiess, H. W. *Multidimensional Solid State NMR and Polymers*; Academic Press: New York, 1994.
(10) Emsley, L.; Laws, D. D.; Pines, A. Lectures on Pulsed NMR (3rd ed.) In *The Proceedings of the International School of Physics "Enrico Fermi"*, Course CXXXIX; Maraviglia, B., Ed.; IOS Press: Amsterdam, 1999; p 45.
(11) Bennett, A. E.; Griffin, R. G.; Vega, S. In *NMR Basic Principles and Progress*; Springer-Verlag: Berlin, 1994; Vol. 33, p 1.
(12) Dusold, S.; Sebald, A. *Ann. Rep. NMR Spectrosc.* **2000**, *41*, 185.
(13) Gullion, T.; Schaefer, J. *J. Magn. Reson.* **1989**, *81*, 196.
(14) Gullion, T.; Schaefer, J. *Adv. Magn. Reson.* **1989**, *13*, 57.
(15) Gullion, T. *Concepts Magn. Reson.* **1998**, *10*, 277.
(16) Feng, X.; Lee, Y. K.; Sandstrøm, D.; Edén, M.; Maisel, H.; Sebald, A.; Levitt, M. H. *Chem. Phys. Lett.* **1996**, *257*, 314.
(17) Hong, M.; Gross, J. D.; Griffin, R. G. *J. Phys. Chem. B* **1997**, *101*, 5869.
(18) Jakobsen, H. J. *Encyclopedia of Nuclear Magnetic Resonance*; Grant, D. M., Harris, R. K., Eds.; Wiley: Chichester, 1996; Vol. 1, p 398.
(19) Samoson, A.; Tuherm, T. *The Alpine Conference on Solid-State NMR*; Chamonix, France, 1999.
(20) Schnell, I.; Lupulescu, A.; Hafner, S.; Demco, D. E.; Spiess, H. W. *J. Magn. Reson.* **1998**, *133*, 61.
(21) Schnell, I.; Brown, S. P.; Low, H. Y.; Ishida, H.; Spiess, H. W. *J. Am. Chem. Soc.* **1998**, *120*, 11784.
(22) Brown, S. P.; Schnell, I.; Brand, J. D.; Müllen, K.; Spiess, H. W. *J. Am. Chem. Soc.* **1999**, *121*, 6712.
(23) Gil, A. M.; Lopes, M. H.; Neto, C. P.; Rocha, J. *Solid State Nucl. Magn. Reson.* **1999**, *15*, 59.
(24) Brown, S. P.; Schnell, I.; Brand, J. D.; Müllen, K.; Spiess, H. W. *J. Mol. Struct.* **2000**, *521*, 179.
(25) Brown, S. P.; Schnell, I.; Brand, J. D.; Müllen, K.; Spiess, H. W. *Phys. Chem. Chem. Phys.* **2000**, *2*, 1735.
(26) Rodriguez, L. N. J.; De Paul, S. M.; Barrett, C. J.; Reven, L.; Spiess, H. W. *Adv. Mater.* **2000**, *12*, 1934.
(27) Ishii, Y.; Tycko, R. *J. Magn. Reson.* **2000**, *142*, 199.
(28) Yamauchi, K.; Kuroki, S.; Fujii, K.; Ando, I. *Chem. Phys. Lett.* **2000**, *324*, 435.
(29) Brown, S. P.; Schaller, T.; Seelbach, U. P.; Koziol, F.; Ochsenfeld, C.; Klärner, F.-G.; Spiess, H. W. *Angew. Chem., Int. Ed. Engl.* **2001**, *40*, 717.
(30) Brown, S. P.; Zhu, X. X.; Saalwächter, K.; Spiess, H. W. *J. Am. Chem. Soc.* **2001**, *123*, 4275.
(31) Van Rossum, B.-J.; Förster, H.; De Groot, H. J. M. *J. Magn. Reson.* **1997**, *124*, 516.
(32) Lesage, A.; Sakellariou, D.; Steuernagel S.; Emsley, L. *J. Am. Chem. Soc.* **1998**, *120*, 13194.
(33) Saalwächter, K.; Graf, R.; Spiess, H. W. *J. Magn. Reson.* **1999**, *140*, 471.
(34) Geen, H.; Titman, J. J.; Gottwald, J.; Spiess, H. W. *Chem. Phys. Lett.* **1994**, *227*, 79.
(35) Geen, H.; Titman, J. J.; Gottwald, J.; Spiess, H. W. *J. Magn. Reson.* **1995**, *A 114*, 264.
(36) Gottwald, J.; Demco, D. E.; Graf R.; Spiess, H. W. *Chem. Phys. Lett.* **1995**, *243*, 314.
(37) Fechtenkötter, A.; Saalwächter, K.; Harbison, M. A.; Müllen, K.; Spiess, H. W. *Angew. Chem., Int. Ed. Engl.* **1999**, *38*, 3039.
(38) Hohwy, M.; Jaroniec, C. P.; Reif, B.; Rienstra, C. M.; Griffin, R. G. *J. Am. Chem. Soc.* **2000**, *122*, 3218.
(39) McElheny, D.; DeVita, E.; Frydman, L. *J. Magn. Reson.* **2000**, *143*, 321.
(40) van Rossum, B.-J.; de Groot, C. P.; Ladizhansky, V.; Vega, S.; de Groot, H. J. M. *J. Am. Chem. Soc.* **2000**, *122*, 3465.
(41) Frydman, L.; Harwood, J. S. *J. Am. Chem. Soc.* **1995**, *117*, 5367.
(42) Gérardy-Montouillout, V.; Malveau, C.; Tekeley, P.; Olender, Z.; Luz, Z. *J. Magn. Reson. A* **1996**, *123*, 7.
(43) Reichert, D.; Zimmermann, H.; Tekeley, P.; Poupko, R.; Luz, Z. *J. Magn. Reson.* **1997**, *125*, 245.
(44) deAzevedo, E. R.; Hu, W.-G.; Bonagamba, T. J.; Schmidt-Rohr, K. *J. Am. Chem. Soc.* **1999**, *121*, 8411.
(45) deAzevedo, E. R.; Hu, W.-G.; Bonagamba, T. J.; Schmidt-Rohr, K. *J. Chem. Phys.* **2000**, *112*, 8988.
(46) Harris, R. K. *Encyclopedia of Nuclear Magnetic Resonance*; Grant, D. M., Harris, R. K., Eds.; Wiley: Chichester, 1996; Vol. 5, p 3301.
(47) Baum, J.; Munowitz, M.; Garroway, A. N.; Pines, A. *J. Chem. Phys.* **1985**, *83*, 2105.
(48) Baum, J.; Pines, A. *J. Am. Chem. Soc.* **1986**, *108*, 7447.
(49) Andrew, E. R.; Bradbury, A.; Eades, R. G. *Nature* **1958**, *182*, 1659.
(50) Lowe, I. *Phys. Rev. Lett.* **1959**, *2*, 285.
(51) Hartmann, S. R.; Hahn, E. L. *Phys. Rev.* **1962**, *128*, 2042.
(52) Pines, A.; Gibby, M. G.; Waugh, J. S. *J. Chem. Phys.* **1972**, *56*, 1776.
(53) Schaefer, J.; Stejskal, E. O. *J. Am. Chem. Soc.* **1976**, *98*, 1031.
(54) Maricq, M. M.; Waugh, J. S. *J. Chem. Phys.* **1979**, *70*, 3300.
(55) Herzfeld, J.; Berger, A. E. *J. Chem. Phys.* **1980**, *73*, 6021.
(56) Filip, C.; Hafner, S.; Schnell, I.; Demco, D. E.; Spiess, H. W. *J. Chem. Phys.* **1999**, *110*, 423.
(57) Scheler, U. *Solid State Nucl. Magn. Reson.* **1998**, *12*, 9.
(58) Waugh, J. S.; Huber, L. M.; Haeberlen, U. *Phys. Rev. Lett.* **1968**, *20*, 180.
(59) Haeberlen, U.; Waugh, J. S. *Phys. Rev.* **1968**, *175*, 453.
(60) Gerstein, B. C.; Pembleton, R. G.; Wilson, R. C.; Ryan, L. M. *J. Chem. Phys.* **1977**, *66*, 361.
(61) Scheler, G.; Haubenreisser, U.; Rosenberger, H. *J. Magn. Reson.* **1981**, *44*, 134.
(62) Maciel, G. E.; Bronnimann, C. E.; Hawkins, B. *Adv. Magn. Reson.* **1990**, *14*, 125.
(63) Dec, S. F.; Bronnimann, C. E.; Wind, R. A.; Maciel, G. E. *J. Magn. Reson.* **1989**, *82*, 454.
(64) Hohwy, M.; Rasmussen, J. T.; Bower, P. V.; Jakobsen, H. J.; Nielsen, N. C. *J. Magn. Reson.* **1998**, *133*, 374.
(65) Hafner, S.; Spiess, H. W. *J. Magn. Reson. A* **1996**, *121*, 160.
(66) Hafner, S.; Spiess, H. W. *Solid State Nucl. Magn. Reson.* **1997**, *8*, 17.
(67) Hafner, S.; Spiess, H. W. *Concepts in Magn. Reson.* **1998**, *10*, 99.
(68) Filip, C.; Hafner, S. *J. Magn. Reson.* **2000**, *147*, 250.
(69) Haeberlen, U. *Adv. Magn. Reson. Suppl.1*; Academic Press: San Diego, 1976.
(70) Lee, M.; Goldburg, W. I. *Phys. Rev. A* **1965**, *140*, 1261.
(71) Bielecki, A.; Kolbert, A. C.; Levitt, M. H. *Chem. Phys. Lett.* **1989**, *155*, 341.
(72) Bielecki, A.; Kolbert, A. C.; de Groot, H. J. M.; Griffin, R. G.; Levitt, M. H. *Adv. Magn. Reson.* **1990**, *14*, 111.
(73) Levitt, M. H.; Kolbert, A. C.; Bielecki, A.; Ruben, D. J. *Solid State Nucl. Magn. Reson.* **1993**, *2*, 151.
(74) Lesage, A.; Steuernagel, S.; Emsley, L. *J. Am. Chem. Soc.* **1998**, *120*, 7095.
(75) Charmont, P.; Lesage, A.; Steuernagel, S.; Engelke, F.; Emsley, L. *J. Magn. Reson.* **2000**, *145*, 334.
(76) Vinogradov, E.; Madhu, P. K.; Vega, S. *Chem. Phys. Lett.* **1999**, *314*, 443.
(77) Vinogradov, E.; Madhu, P. K.; Vega, S. *Chem. Phys. Lett.* **2000**, *329*, 207.
(78) Lesage, A.; Duma, L.; Sakellariou, D.; Emsley, L. *J. Am. Chem. Soc.* **2001**, *123*, 5747.
(79) Bodenhausen, G.; Kogler, H.; Ernst, R. R. *J. Magn. Reson.* **1984**, *58*, 370.
(80) Hore, P. J.; Jones, J. A.; Wimperis, S. *NMR: The Toolokit*; Oxford University Press: Oxford, 2000.
(81) Sørensen, O. W.; Rance, M.; Ernst, R. R. *J. Magn. Reson.* **1984**, *56*, 527.
(82) Sakellariou, D.; Lesage, A.; Hodgkinson, P.; Emsley, L. *Chem. Phys. Lett.* **2000**, *319*, 253.
(83) Schnell, I.; Spiess, H. W. *J. Magn. Reson.* **2001**, *151*, 153.
(84) Bodenhausen, G. *Prog. NMR Spectrosc.* **1981**, *14*, 137.
(85) Weitekamp, D. P. *Adv. Magn. Reson.* **1983**, *11*, 111.
(86) Norwood, T. J. *Prog. NMR Spectrosc.* **1992**, *24*, 295.
(87) Marion, D.; Wüthrich, K. *Biochem. Biophys. Res. Commun.* **1983**, *113*, 967.
(88) Marion, D.; Ikura, M.; Tschudin, R.; Bax, A. *J. Magn. Reson.* **1989**, *85*, 393.

(89) Meier, B. H.; Earl, W. L. *J. Chem. Phys.* **1986**, *85*, 4905.
(90) Meier, B. H.; Earl, W. L. *J. Am. Chem. Soc.* **1987**, *109*, 7937.
(91) Sommer, W.; Gottwald, J.; Demco, D. E.; Spiess, H. W. *J. Magn. Reson.* **1995**, *A 113*, 131.
(92) Lee, Y. K.; Kurur, N. D.; Helmle, M.; Johannessen, O. G.; Nielsen, N. C.; Levitt, M. H. *Chem. Phys. Lett.* **1995**, *242*, 304.
(93) Tycko, R.; Dabbagh, G. *J. Am. Chem. Soc.* **1991**, *113*, 9444.
(94) Gregory, D. M.; Wolfe, G.; Jarvie, T.; Shiels, J. C.; Drobny, G. P. *Mol. Phys.* **1996**, *89*, 1835.
(95) Nielsen, N. C.; Bildsøe, H.; Jakobsen, H. J.; Levitt, M. H. *J. Chem. Phys.* **1994**, *101*, 1805.
(96) Brinkmann, A.; Edén, M.; Levitt, M. H. *J. Chem. Phys.* **2000**, *112*, 8539.
(97) Carravetta, M.; Edén, M.; Zhao, X.; Brinkmann, A.; Levitt, M. H. *Chem. Phys. Lett.* **2000**, *321*, 205.
(98) Feike, M.; Demco, D. E.; Graf, R.; Gottwald, J.; Hafner, S.; Spiess, H. W. *J. Magn. Reson.* **1996**, *A 122*, 214.
(99) Graf, R.; Demco, D. E.; Gottwald, J.; Hafner, S.; Spiess, H. W. *J. Chem. Phys.* **1997**, *106*, 885.
(100) Caravetti, P.; Neuenschwander, P.; Ernst, R. R. *Macromolecules* **1985**, *18*, 119.
(101) Feike, M.; Graf, R.; Schnell, I.; Jäger, C.; Spiess, H. W. *J. Am. Chem. Soc.* **1996**, *118*, 9631.
(102) Dollase, W. A.; Feike, M.; Förster, H.; Schaller, T.; Schnell, I.; Sebald, A. Steuernagel, S. *J. Am. Chem. Soc.* **1997**, *119*, 3807.
(103) Geen, H.; Gottwald, J.; Graf, R.; Schnell, I.; Spiess, H. W.; Titman, J. J. *J. Magn. Reson.* **1997**, *125*, 224.
(104) Witter, R.; Hartmann, P.; Vogel, J.; Jäger, C. *Solid State Nucl. Magn. Reson.* **1998**, *13*, 189.
(105) Schemdt auf der Günne, J.; Eckert, H. *Chem. Eur. J.* **1998**, *4*, 1762.
(106) Nielsen, N. C.; Creuzet, F.; Griffin, R. G.; Levitt, M. H. *J. Chem. Phys.* **1992**, *96*, 5668.
(107) Hong, M. *J. Magn. Reson.* **1999**, *136*, 86.
(108) Bax, A.; Freeman, R.; Frenkiel, T. A. *J. Am. Chem. Soc.* **1981**, *103*, 2102.
(109) Wüthrich, K. *NMR of Proteins and Nucleic Acids*; Wiley: New York, 1986.
(110) Lesage, A.; Auger, C.; Caldarelli, S.; Emsley, L. *J. Am. Chem. Soc.* **1997**, *119*, 7867.
(111) Lesage, A.; Bardet, M.; Emsley, L. *J. Am. Chem. Soc.* **1999**, *121*, 10987.
(112) Schmidt-Rohr, K.; Hu, W.; Zumbulyadis, N. *Science* **1998**, *280*, 714.
(113) Friedrich, U.; Schnell, I.; Brown, S. P.; Lupulescu, A.; Demco, D. E.; Spiess, H. W. *Mol. Phys.* **1998**, *95*, 1209.
(114) Hodgkinson, P.; Emsley, L. *J. Magn. Reson.* **1999**, *139*, 46.
(115) Tekeley, P.; Demco, D. E.; Canet, D.; Malveau, C. *Chem. Phys. Lett.* **1999**, *309*, 101.
(116) De Paul, S. M.; Saalwächter, K.; Graf, R.; Spiess, H. W. *J. Magn. Reson.* **2000**, *146*, 140.
(117) Gregory, D. M.; Metha, M. A.; Shiels, J. C.; Drobny, G. P. *J. Chem. Phys.* **1997**, *107*, 28.
(118) Caravatti, P.; Bodenhausen, G.; Ernst, R. R. *Chem. Phys. Lett.* **1982**, *89*, 363.
(119) Caravatti, P.; Braunschweiler, L.; Ernst, R. R. *Chem. Phys. Lett.* **1983**, *100*, 305.
(120) Bronnimann, C. E.; Ridenour, C. F.; Kinney, D. R.; Maciel, G. E. *J. Magn. Reson.* **1992**, *97*, 522.
(121) Gu, Z.; Ridenour, C. F.; Bronnimann, C. E.; Iwashita, T.; McDermott, A. *J. Am. Chem. Soc.* **1996**, *118*, 822.
(122) Schmidt-Rohr, K.; Clauss, J.; Spiess, H. W. *Macromolecules* **1992**, *25*, 3273.
(123) Mirau, P. A.; Heffner, S. A.; Schilling, M. *Solid State Nucl. Magn. Reson.* **2000**, *16*, 47.
(124) Lesage, A.; Charmont, P.; Steuernagel, S.; Emsley, L. *J. Am. Chem. Soc.* **2000**, *122*, 9739.
(125) Saalwächter, K.; Graf, R.; Spiess, H. W. *J. Magn. Reson.* **2001**, *148*, 398.
(126) Metz, G.; Wu, X.; Smith, S. O. *J. Magn. Reson. A* **1994**, *110*, 219.
(127) Bodenhausen, G.; Ruben, D. J. *Chem. Phys. Lett.* **1980**, *69*, 185.
(128) Müller, L. *J. Am. Chem. Soc.* **1979**, *101*, 4481.
(129) Bennett, A. E.; Rienstra, C. M.; Auger, M.; Lakshmi, K. V.; Griffin, R. G. *J. Chem. Phys.* **1995**, *103*, 6951.
(130) Ernst, M.; Zimmermann, H.; Meier, B. H. *Chem. Phys. Lett.* **2000**, *317*, 581.
(131) Lesage, A.; Emsley, L. *J. Magn. Reson.* **2001**, *148*, 449.
(132) Spiess, H. W. *Chem. Rev.* **1991**, *91*, 1321.
(133) Hester, R. K.; Ackerman, J. L.; Neff, B. L.; Waugh, J. S. *Phys. Rev. Lett.* **1976**, *36*, 1081.
(134) Munowitz, M. G.; Griffin, R. G.; Bodenhausen, G. Huang, T. H. *J. Am. Chem. Soc.* **1981**, *103*, 2529.
(135) Munowitz, M. G.; Griffin, R. G. *J. Chem. Phys.* **1982**, *76*, 2848.
(136) Roberts, J. E.; Harbison, G. S.; Munowitz, M. G.; Herzfeld, J.; Griffin, R. G. *J. Am. Chem. Soc.* **1987**, *109*, 4163.
(137) Saalwächter, K.; Spiess, H. W. *J. Chem. Phys.* **2001**, *114*, 5707.
(138) Jeffrey, G. A.; Saenger, W. *Hydrogen Bonding in Biological Structures*; Springer-Verlag: New York, 1991.
(139) Gann, S. L.; Baltisberger, J. H.; Pines, A. *Chem. Phys. Lett.* **1994**, *210*, 405.
(140) Alderman, D. W.; McGeorge, G.; Hu, J. Z.; Pugmire, R. J.; Grant, D. M. *Mol. Phys.* **1998**, *95*, 1113.
(141) Gan, Z. *J. Am. Chem. Soc.* **1992**, *114*, 8307.
(142) Harper, J. K.; Grant, D. M. *J. Am. Chem. Soc.* **2000**, *122*, 3708.
(143) Berglund, B.; Vaughan, R. W. *J. Chem. Phys.* **1980**, *73*, 2037.
(144) Jeffrey, G. A.; Yeon, Y. *Acta Crystallogr.* **1986**, *B42*, 410.
(145) Harris, R. K.; Jackson, P.; Merwin, L. H.; Say, B. J.; Hagele, G. *J. Chem. Soc., Faraday Trans.* **1988**, *84*, 3649.
(146) Ning, X.; Ishida, H. *J. Polym. Sci. Chem. Ed.* **1994**, *32*, 1121.
(147) Ishida, H.; Allen, D. J. *J. Polym. Sci. Phys. Ed.* **1996**, *34*, 1019.
(148) Shen, S. B.; Ishida. H. *Polym. Composites* **1996**, *17*, 710.
(149) Ishida, H.; Low, H. Y. *Macromolecules* **1997**, *30*, 1099.
(150) Wirasate, S.; Dhumrongvaraporn, S.; Allen, D. J.; Ishida, H. *J. Appl. Polym. Sci.* **1998**, *70*, 1299.
(151) Dunkers, J.; Zarate, E. A.; Ishida, H. *J. Phys. Chem.* **1996**, *100*, 13514.
(152) Schnell, I.; Langer, B.; Söntjens, S. H. M.; van Genderen, M. H. P.; Sijbesma, R. P.; Spiess, H. W. *J. Magn. Reson.* **2001**, *150*, 57.
(153) Shantz, D. F.; Schmedt auf der Günne, J.; Koller, H.; Lobo, R. F. *J. Am. Chem. Soc.* **2000**, *122*, 6659.
(154) McDonagh, A. F. Bile Pigments: Bilatrienes and 5, 15-Biladienes. In *The Porphyrins*; Dolphin, D., Ed.; Acdemic Press: New York, 1979; Vol. VI, Chapter 6.
(155) Chowdhury, J. R.; Wolkoff, A. S.; Chowdhury, N. R.; Arias, I. M. In *The Metabolic and Molecular Bases of Inherited Diseases*; Scriver, C. R., Beaudet, A. L., Sly, W. S., Valle, D., Eds.; McGraw-Hill: New York, 1995; Vol. II, pp 2161−2208.
(156) Bonnett, R.; Davies, J. E.; Hursthouse, M. B. *Nature* **1976**, *262*, 326.
(157) Le Bas, G.; Allegret, A.; Mauguen, Y.; de Rango, C.; Bailly, M. *Acta Crystallogr.* **1980**, *B36*, 3007.
(158) Henry, E. R.; Szabo, A. *J. Chem. Phys.* **1985**, *82*, 4753.
(159) Lazzeretti, P. *Prog. NMR Spectrosc.* **2000**, *36*, 1.
(160) Waugh, J. S.; Fessenden, R. W. *J. Am. Chem. Soc.* **1956**, *79*, 846.
(161) van Rossum, B.-J.; Boender, G. J.; Mulder, F. M.; Raap, J.; Balaban, T. S.; Holzwarth, A.; Schaffner, K.; Prytulla, S.; Oschkinat, H.; de Groot, H. J. M. *Spectrochim. Acta* **1998**, *A54*, 1167.
(162) van Rossum, B.-J.; Steensgaard, D. B.; Mulder, F. M.; Boender, G. J.; Schaffner, K.; Holzwarth, A. R.; de Groot, H. J. M. *Biochemistry* **2001**, *40*, 1587.
(163) Watson, M. D.; Fechtenkötter, A.; Müllen, K. *Chem. Rev.* **2001**, *101*, 1267.
(164) Goddard, R.; Haenel, M. W.; Herndon, W. C.; Krüger, C.; Zander, M. *J. Am. Chem. Soc.* **1995**, *117*, 30.
(165) Gauss, J. *Ber. Bunsen-Ges. Phys. Chem.* **1995**, *99*, 1001.
(166) de Dios, A. C. *Prog. NMR Spectrosc.* **1996**, *29*, 229.
(167) Bühl, M. Structural Applications of NMR Chemical Shift Computations In *Encyclopedia of Computational Chemistry*; von Ragué Schleyer, P., Allinger, N. L., Clark, T., Gastgeiger, J., Kollman, P. A., Schaefer, H. F., III, Schreiner, P. R., Eds.; Wiley: Chichester, 1998; p 1835.
(168) Ochsenfeld, C.; Brown, S. P.; Schnell, I.; Gauss, J.; Spiess, H. W. *J. Am. Chem. Soc.* **2001**, *123*, 2597.
(169) Ochsenfeld, C. *Phys. Chem. Chem. Phys.* **2000**, *2*, 2153.
(170) Klärner, F.-G.; Benkhoff, J.; Boese, R.; Burkert, U.; Kamieth, M.; Naatz, U. *Angew. Chem., Int. Ed. Engl.* **1996**, *35*, 1130.
(171) Klärner, F.-G.; Burkert, U.; Kamieth, M.; Boese, R.; Benet-Buchholz, J. *Chem. Eur. J.* **1999**, *5*, 1700.
(172) Graf, R.; Heuer, A.; Spiess, H. W. *Phys. Rev. Lett.* **1998**, *80*, 5738.
(173) Dollase, T.; Graf, R.; Heuer, A.; Spiess, H. W. *Macromolecules* **2001**, *34*, 298.
(174) Graf, R.; Demco, D. E.; Hafner, S.; Spiess, H. W. *Solid State Nucl. Magn. Reson.* **1998**, *12*, 139.
(175) Langer, B.; Schnell, I.; Spiess, H. W.; Grimmer, A.-R. *J. Magn. Reson.* **1999**, *138*, 182.
(176) Günther, H. *NMR−Spektroskopie*; Thieme Verlag: Stuttgart, 1992; p. 310 (eqs 9.11 and 9.12).
(177) Stöckli, A.; Meier, B. H.; Kreis, R.; Meyer, R.; Ernst, R. R. *J. Chem. Phys.* **1990**, *93*, 1502.
(178) Anulewicz, R.; Wawer, I.; Krygowski, T. M.; Männle, F.; Limbach H.-H. *J. Am. Chem. Soc.* **1997**, *119*, 12223.
(179) Takeda, S.; Inabe, T.; Benedict, C.; Langer, U.; Limbach, H.-H. *Ber. Bunsen-Ges. Phys. Chem.* **1998**, *102*, 1358.
(180) Herwig, P.; Kayser, C. W.; Müllen, K.; Spiess, H. W. *Adv. Mater.* **1996**, *8*, 510.
(181) van de Craats, A. M.; Warman, J. M.; Fechtenkötter, A.; Brand, J. D.; Harbison M. A.; Müllen, K. *Adv. Mater.* **1999**, *11*, 1469.
(182) Demus, D.; Goodby, J. W.; Gray, G. W.; Spiess, H. W.; Vill, V., Eds. *Handbook of Liquid Crystals*; Wiley-VCH: Weinheim, 1998.
(183) Abragam, A. *The Principles of Nuclear Magnetism*; Clarendon: Oxford, 1961.
(184) Wind, M.; Wiesler, U.-M.; Saalwächter, K.; Müllen, K.; Spiess, H. W. *Adv. Mater.* **2001**, *13*, 752.

CR990132E